II.2

Lithostratigraphic characterization of the Abrantes region (Central Portugal); the Cadomian to Variscan Cycle transition in the Ossa-Morena Zone

Index

II.2.1. Introduction

The Iberian Massif (IM) represents the western edge of the European Variscan Chain and the lithostratigraphic record, from Neoproterozoic to Palaeozoic, reflecting a long-lasting geodynamic evolution correlative of two orogenic cycles: Cadomian and Variscan (*e.g.* Eguíluz *et al.*, 2000; Simancas *et al.*, 2004; Ribeiro *et al.*, 2007; 2009). The recognition of stratigraphic, structural, magmatic and metamorphic contrasting features allowed the subdivision of IM into different tectonostratigraphic zones. The early IM subdivision proposal is due by Lötze (1945) and afterwards other proposals are established (*e.g.* Julivert *et al.*, 1974; Ribeiro *et al.*, 1979; 1990; Quesada, 1991), however, no significantly changes for the foremost boundaries are done (Fig. 1A).

During Upper Neoproterozoic times, the Ossa-Morena Zone (OMZ) and Central Iberian Zone (CIZ) underwent distinct geodynamic evolution, as recorded by its distinct geological record. The boundary between these tectonostratigraphic zones is marked by a lithospheric shear zone, known as the Tomar-Badajoz-Cordoba Shear Zone (TBCSZ; Fig. 1A), which some authors consider a Cadomian suture (*e.g*. Ribeiro *et al.*, 2007; 2009). This shear zone includes strongly dismembered and retrograded eclogite lenses, granulites and gneisses with Neoproterozoic age (Quesada, 1991; Abalos *et al.*, 1992; Pereira *et al.*, 2006; 2010a; Ribeiro *et al.*, 2009; Henriques *et al.*, 2015), recording its polycyclic evolution. Although other authors (e.g. Linnemann *et al.*, 2008; Sanchez-Lorda *et al.* 2014; Eguiluz *et al.*., 2016) propose that the Cadomian suture was located at south of the OMZ (current coordinates), removing importance to the TBCSZ during Cadomian Cycle.

During Early Cambrian times, the OMZ and CIZ shared a common geodynamic evolution, controlled by the first stages of Variscan Cycle, however with their own features (*e.g.* Pereira *et al.*, 2006; Ribeiro *et al.*, 2007; 2009; Linnemann *et al.*, 2008; Sanchez-Garcia *et al.*, 2010). The intracontinental rifting onset, which culminate with a Variscan Ocean opening at southwest of OMZ (*e.g.* Ribeiro *et al.*, 2007; Pedro *et al.*, 2010; Sanchez-Garcia *et al.*, 2010; Moreira *et al.*, 2014a), led to the development of a set of individual basins with peculiar stratigraphic features (Oliveira *et al.*, 1991; Etxebarria *et al.*, 2006; Araújo *et al.*, 2013).

The Abrantes region was affected by intense tectono-metamorphic events during Variscan and Cadomian Cycles and the reconstruction of lithostratigraphic succession is crucial to understand the geodynamical evolution of these area. In addition, the relevance of this region relies on its location, neighbouring the OMZ and CIZ. In fact, the detailed characterization of the lithostratigraphic succession recognised in the Abrantes region supports its affinity with the OMZ sequences developed throughout the Neoproterozoic-Cambrian transition. There is no evidence to support any kind of correlation with geological units of the CIZ. This study shows the lithostratigraphic affinity of defined succession with the Neoproterozoic-Cambrian successions of OMZ, based on comprehensive lithostratigraphic and geochemical characterization, extending the OMZ until Abrantes region as initially proposed by Romão *et al.* (2010; 2014).

II.2.2. Geological setting

The Abrantes region is a key sector of the SW Iberian Variscides, offering the possibility to characterize in detail the spatial arrangement and the interference patterns related to the convergence of two first-order shear zones: the Porto-Tomar-Ferreira do Alentejo (PTFASZ), with right-lateral kinematics, and the TBCSZ, described as a sinistral transpressive shear zone

(Fig. 1). The comprehensive lithostratigraphic succession analysis is a critical step to improve significantly the current understanding of the role played by PTFASZ and TBCSZ during decisive timeframes of the geodynamic evolution occurred in Neoproterozoic-Cambrian transition times, but also during the Upper Palaeozoic times.

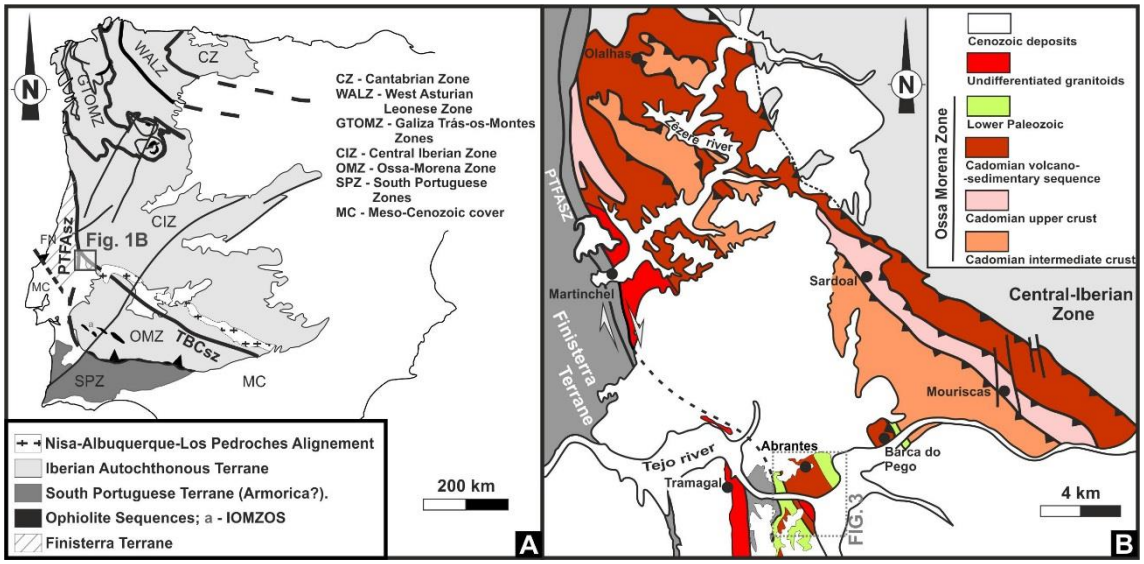

Figure 1 – Geographic and geological settings:

A – Subdivision of the Iberian Massif in tectonostratigraphic zones (modified from, e.g., Julivert *et al.*, 1974; Ribeiro *et al.*, 1990; Quesada, 1991);

B – Simplified geological map of the Tomar-Abrantes region, showing the fundamental tectonostratigraphic succession proposed by Romão *et al.* (2010), with the location of study area.

The stratigraphic sequence observed in Abrantes, devoid of fossil content and recrystallized under Greenschist to Amphibolitic metamorphic conditions (Moreira, 2012), was early considered as Proterozoic (Gonçalves *et al.,* 1979; Teixeira, 1981). The authors highlights its macroscopic resemblance with the *Série Negra* (Black Series) of OMZ. However, preliminary works (e.g. Romão *et al.,* 2010; Moreira *et al.*, 2015) show that it is possible to distinguish a typical OMZ Neoproterozoic-Cambrian succession. A tectonostratigraphic succession was proposed by Romão *et al.* (2010) for the Tomar-Abrantes region (Fig. 1B):

- A Cadomian Middle Crust composed of retrogressed granulites developed in the course of a high grade metamorphic event peaking at 539 ± 3 Ma (Henriques *et al.*, 2009) and involving a Neoproterozoic protolith;

- A Cadomian Upper Crust composed of gneissic granites with Neoproterozoic age (569±3 Ma, U-Pb in zircons; Henriques *et al.*, 2015) and metamorphosed during the Neoproterozoic-Cambrian times (ca. 545 Ma, U-Pb in monazites; Henriques *et al.*, 2015);

- A Cadomian volcano-sedimentary sequence composed of phyllites and meta-greywackes recrystallized under greenschist facies conditions, interbedded with black cherts and bimodal meta-volcanic rocks, included in the *Série Negra* Group;

- An Early Palaeozoic succession (Cambrian to Silurian) composed of bimodal meta-volcanic rocks, marbles and meta-arkoses, presenting similarities with the OMZ successions.

According to Romão *et al.* (2010), the stratigraphic succession observed in Abrantes region is composed of a Cadomian volcano-sedimentary sequence overlaid by an Early Palaeozoic cover (Fig. 1B). The lowermost units, representing the Cadomian Middle and Upper crust, only can be observed in the eastern sections of the study area (Fig. 1B).

II.2.3. Synopsys of Neoproterozoic-Cambrian successions of OMZ

The OMZ stratigraphy is usually organized in domains or sectors, emphasizing the particular stratigraphic features presented by small basins generated during the early Palaeozoic crustal thinning (e.g. Liñan and Quesada, 1990; Oliveira *et al.*, 1991; Gozalo *et al.*, 2003; Etxebarria *et al.*, 2006; Araújo *et al.*, 2013). Following, a summary of the regional Neoproterozoic and Cambrian stratigraphic characteristics can be attempted, highlighting, when necessary, the specific features recognized in some domains (Fig. 2).

II.2.3.1. Neoproterozoic succession

The OMZ stratigraphic succession begins with units assigned to the Neoproterozoic, usually forming the core of NW-SE oriented structures. From north to south, these units have been described: (1) the northern edge of the OMZ, outlined by TBCSZ and the Obejo-Valsequillo-Puebla de la Reina Domain (Apalategui *et al.*, 1990); (2) the core of the Estremoz, Olivenza-Monesterio and Vila Boim-Elvas Antiforms located in Central OMZ; and (3) in the Almadén de la Plata-Aracena and Montemor-o-Novo regions and in the core of the Moura, Viana do Alentejo and Serpa Antiforms, in the OMZ Southern Domains (*e.g.* Quesada *et al.*, 1990; Oliveira *et al.*, 1991; Eguilluz *et al.*, 2000; Lopes, 2003; Pereira *et al.*, 2006; 2012a; Araújo *et al.*, 2013; Moreira *et al.*, 2014b). Despite of local labelling, all these units are commonly included the *Série Negra* Group, formally described in Portugal by Carvalhosa (1965) and in Spain by Alia (1963) and Vegas (1968).

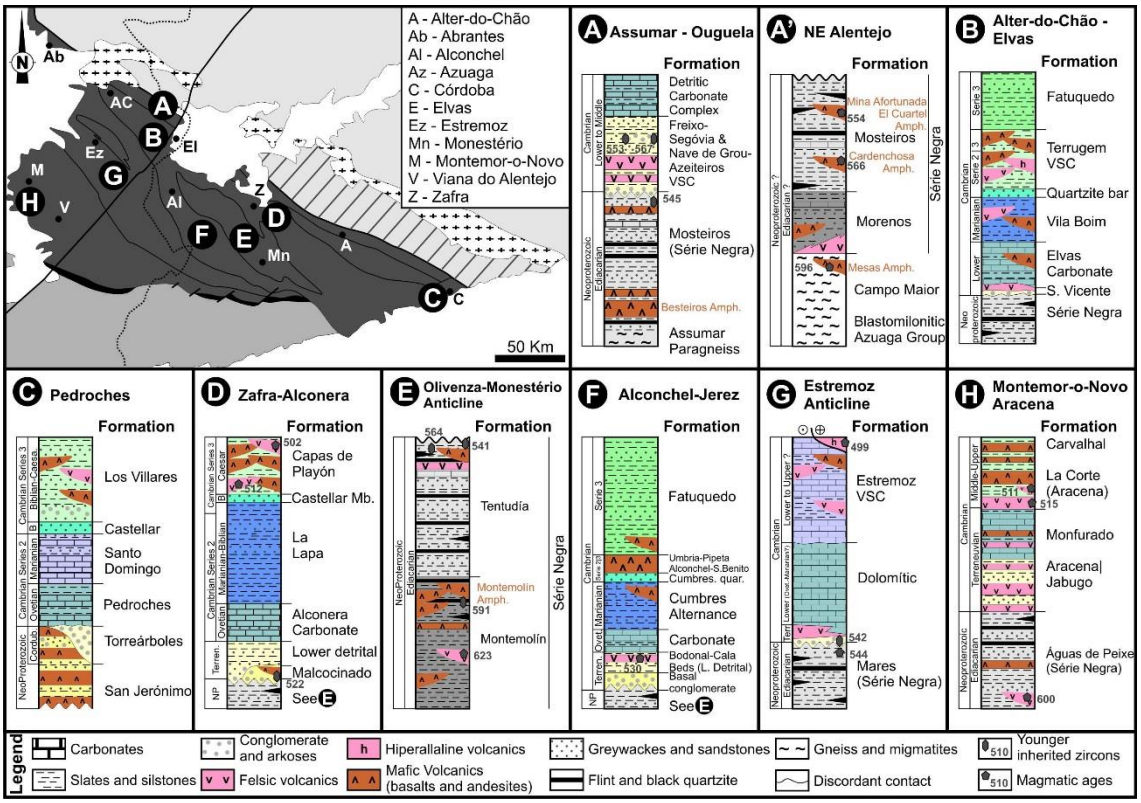

Figure 2 – Neoproterozoic-Cambrian lithostratigraphic columns of the OMZ and their location in a simplified subdivision map of OMZ proposed by Apalategui *et al.* (1990) (Columns and geochronological data adapted from: (A) Pereira *et al.*, 2006; Linnemann *et al.*, 2008; (A') – Oliveira *et al.*, 1991; Ordóñez-Casado, 1998; (B) Oliveira *et al.*, 1991; Moreira *et al.*, 2014b; (C) Ordóñez-Casado, 1998; Gozalo *et al.*, 2003; Creveling *et al.*, 2013; (D) Gozalo *et al.*, 2003; Vera, 2004; Etxebarria *et al.*, 2006; Sanchez-Gárcia *et al.*, 2010; (E) Eguíluz *et al.*, 1990; Schafer *et al.*, 1993; Fernandez-Suarez *et al.*, 2002; Vera, 2004; Sanchez-Garcia *et al.*, 2007; Ordoñez-Casado *et al.*, 2009; (F) Etxebarria *et al.*, 2006; Romeo *et al.*, 2006; Sanchez-Gárcia *et al.*, 2010; (G) Coelho and Gonçalves, 1970; Oliveira *et al.*, 1991; Pereira *et al.*, 2012a (H) Oliveira *et al.*, 1991; Ordóñez-Casado, 1998; Pereira *et al.*, 2006; Chichorro *et al.*, 2008).

In the Portuguese segment of the TBCSZ (NE Alentejo), Oliveira *et al.* (1991) describe a basal unit, beneath *Série Negra* Group, comprising moderately to strongly retrograded high-grade metamorphic rocks, namely felsic (ortho)gneisses and migmatites, associated with mafic granulites and locally including eclogite lenses (Campo Maior Formation; Fig. 2). Recent geochronological data (Pereira *et al.*, 2012b) were interpreted as indicative of an Ordovician age for the protolith of some of this (ortho)gneisses (465 ± 14 Ma; SHRIMP U-Pb in zircon). However, similar high-grade rocks, as Cerro Muriano gneiss (595 ± 30 Ma; K-Ar in feldspar – Bellon *et al.*, 1979), associated to Neoproterozoic ortho-amphibolites are also observed in the Central Unit (*e.g.* Abalos, 1989; 1992; Abalos *et al.*, 1990; 1991), being the age of high-grade metamorphic rocks dubious.

In NE Alentejo, over the basal high-grade unit, two distinct metasedimentary Formations, both included in *Série Negra* Group and recording metamorphic recrystallization under greenschist to amphibolite facies conditions (Fig. 2), was described, from bottom to top (Oliveira *et al.,* 1991):

- Morenos Formation: comprises felsic and mafic meta-volcanic rocks, black metacherts, siliceous shales, meta-arkoses and metapsammites; the top of this sequence is locally traced by calc-silicate rocks and garnet-bearing micaschists.
- Mosteiros Formation: includes a monotonous sequence of black schists, metagreywackes and metapsammites interlayered with black siliceous chemiogenic (metacherts/flints) or siliciclastic fine-grained quartzites and amphibolites (*e.g.* Oliveira *et al.*, 1991; Eguíluz *et al.*, 2000; Oliveira *et al.*, 2003; Araújo *et al.*, 2013; Fig. 2). The bottom of Mosteiros Formation succession comprises a mafic meta-volcanic member with sub-alkaline tholeiitic geochemical signature, labelled as the Besteiros Amphibolites (Ribeiro *et al.*, 2003; Pereira *et al.*, 2006).

Also in the Olivenza-Monesterio Anticline, two distinct lithostratigraphic sequences were identified (*e.g.* Eguíluz *et al.*, 1990; 2000; Vera, 2004; Ordoñez-Casado *et al.*, 2009; Fig. 2), from bottom to top:

- Montemolín Succession: composed of graphite-rich metapelites, meta-quartzwackes and biotite-bearing metapsammites, sometimes also including metagreywackes and meta-arkoses, with lenticular black quartzites, metacarbonates and amphibolites (Eguíluz *et al.*, 1990; 2000; Ordoñez-Casado *et al.*, 2009). The abundance of amphibolites increases to the top of the succession, where an important amphibolite member, with less significant metapelite and metagreywacke series, occurs (the Montemolín Amphibolites; Eguíluz *et al.*, 1990; 2000). Geochemical data in these amphibolites point to a tholeiitic affinity (Eguíluz *et al.*, 1990; Gómez-Pugnaire *et al.*, 2003; Sanchez Lorda *et al.*, 2014). The youngest age of detrital zircons extracted from metapelites on top of the Montemolín Succession indicates a maximum deposition time span around 590-580 Ma (591 ± 11; SHRIMP U-Pb in zircon, Ordoñez-Casado *et al.*, 2009), therefore constraining the depositional age of the this succession.
- Tentudía Succession: apparently in stratigraphic continuity with the Montemolín succession, but records metamorphic recrystallization under lower grade conditions. It comprises essentially a monotonous sequence of black shales, metagreywackes and black quartzites, sporadically with amphibolite lenses and metacarbonates (Eguíluz *et al.*, 1990; 2000; Quesada *et al.*, 1990; Sanchez Lorda *et al.*, 2014). A maximum deposition

age around 540-545 Ma (Ediacarian-Cambrian transition) point to the top of the *Série Negra* Group (*e.g.* Schäfer *et al.*, 1993; Fernandez-Suarez *et al.*, 2002; Chichorro *et al.*, 2008; Linnemann *et al.*, 2008; Pereira *et al.*, 2012a).

The basal section of the Olivenza-Monestério Anticline is rooted in a migmatitic core whose early (prograde) metamorphic path has been assigned to the Lower Palaeozoic geodynamic evolution (Eguíluz *et al.*, 2000; Simancas *et al.*, 2004 and references therein).

The amphibolites within Neoproterozoic successions present tholeiitic (N/E-MORB) to calc-alkaline geochemical affinity and they are interpreted as resulting from volcanic-arc development during Cadomian Cycle (Eguíluz *et al.*, 1990; Gómez-Pugnaire *et al.*, 2003; López-Guijarro *et al.*, 2008; Sanchez Lorda *et al.*, 2014). The available geochronological data for these amphibolites and other volcanic rocks apparently show two distinct steps of volcanic activity:

- ca. 630-600 Ma: 617 ± 6 Ma (U-Pb in zircon; Schäfer *et al.*, 1989) for amphibolites from TBCSZ; 645 ± 17 Ma, 610 ± 13 Ma and 585 ± 8,9 Ma (LA-ICPMS U-Pb in zircon; Sanchez-Lorda *et al.*, 2016), from El Cuartel calc-alkaline amphibolite (northern OMZ); 611 +17/-12 Ma (U-Pb in zircon; Schäfer, 1990) from the Cardenchosilla amphibolites (northern OMZ); 596 ± 14 and 577 ± 26 Ma (SHRIMP U-Pb in zircon; Ordóñez-Casado, 1998) from Las Mesas amphibolites (northern OMZ); 623 ± 3 Ma (TIMS U-Pb zircon; Sanchez-Garcia *et al.*, 2007) from meta-rhyolites of Loma del Aire; 600 ± 13 Ma (SHRIMP U-Pb zircon; Ordóñez-Casado, 1998) from granodiorites in the Lora del Rio region
- ca. 580-545 Ma: 566 ± 9 Ma (SHRIMP U-Pb in zircon, Ordóñez-Casado, 1998) and 567 ± 3 Ma (U-Pb in zircon, Schäfer *et al.*, 1988) and 580 ± 1,4 Ma (LA-ICPMS U-Pb in zircon; Sanchez-Lorda *et al.*, 2016) from La Cardenchosilla E-MORB amphibolites; 554 ± 16 Ma and 549 ± 16 Ma (SHRIMP U-Pb in zircon; Ordóñez-Casado, 1998) from El Cuartel and Calera de León amphibolites respectively; 544.2 ± 1.7 Ma, 544.3 ± 2.5 Ma and 544 ± 2 Ma (SHRIMP U-Pb in zircon; Henriques *et al.*, 2015) from Mouriscas amphibolites; 573 ± 14 Ma (SHRIMP U-Pb zircon; Bandrés *et al.*, 2004) from subvolcanic rocks related to Valle de la Serena granitic porphyry.

Unconformably on top of the Tentudía Succession, it occurs a meta-volcanoclastic sequence comprising andesites, conglomerates, psammites and pellites (Malcocinado and San Jerónimo Formations), being assigned to the Lower Cambrian age (522 ± 8 Ma; maximum age of deposition of siliciclastic series, SHRIMP U-Pb in zircons; Ordonez Casado *et al.*, 1998). The volcanic lithotypes show a calc-alkaline geochemical affinity (Sánchez-Carretero *et al.*, 1990; Pin *et al.*, 2002; Lopez Guijarro *et al.*, 2008). So far, successions alike of the Malcocinado and San Jerónimo Formations were not identified in the OMZ Portuguese segment

Considering the geochronological constraints so far determined, all the aforementioned lithostratigraphic sequences should be developed in the course of the Cadomian Cycle, thus recording the main evolving stages of OMZ during Neoproterozoic times, roughly from 630-530 Ma (Quesada *et al.*, 1990; Eguilluz *et al.*, 2000; Pereira *et al.*, 2006; 2011; Ribeiro *et al.*, 2009; Sanchez Lorda *et al.*, 2014; Henriques *et al.*, 2015).

II.2.3.2. Cambrian succession

The Cambrian succession is unconformably over the Neoproterozoic succession. This succession comprises felsic meta-volcanic rocks, metaconglomerates (including pebbles of early deformed rocks from the *Série Negra* Group), arkosic metasandstones and metapelites (*e.g.* Basal Cambrian Conglomerate, Bodonal-Cala Beds, Torreárboles, S. Vicente, Nave de Grou-Azeiteiros and Freixo-Segóvia Formation; Mata and Munhá 1990; Oliveira *et al.*, 1991; Pereira *et al.*, 2006a; 2012a; Chichorro *et al.*, 2008; Sánchez-García *et al.*, 2010; Fig. 2). Occasionally, some interbedded carbonate rocks occur within sequence, becoming progressively more abundant to the top of the sequence. Geochronological data for detrital zircons from siliciclastic horizons in the Estremoz Anticline and other correlative lithostratigraphic units in the OMZ North domains indicate maximum deposition ages around 530 Ma (Pereira *et al.*, 2006; 2012a; Linnemann *et al.*, 2008). The obtained detrital ages is consistent with magmatic ages obtained in interbedded felsic meta-volcanic rocks ages (530 $\pm$ 3 Ma, U-Pb in zircons; Romeo *et al.*, 2006). These felsic meta-volcanic rocks presents calc-alkaline geochemistry (*e.g.* Ordoñez-Casado *et al.*, 1998; Sanchez-Garcia *et al.*, 2010).

Over the previous described detrital-felsic succession, without stratigraphic unconformity, an extensive carbonate succession comprising a minor volcanic component was developed during Early Cambrian (*e.g*. Mata and Munhá, 1990; Oliveira *et al.*, 1991; Simancas *et al.*, 2004; Etxebarria *et al.*, 2006; Sánchez-García *et al.*, 2010; Moreira *et al.*, 2014b). The carbonate succession (Pedroches, Estremoz Dolomitic, Elvas Carbonated, Alconera and Carvalhal Formations; Fig. 2) includes dolomite-rich and calcite marbles and limestones, besides with occasional siliciclastic beds (*e.g.* Oliveira *et al.*, 1991; Pereira *et al.*, 2006; Chichorro *et al.*, 2008; Creveling *et al.*, 2013). These successions are assigned to Lower Ovetian to Lower Marianian (Cambrian Series 2), based on faunistic associations (*e.g.* Liñan and Quesada, 1990; Oliveira *et al.*, 1991; Gozalo *et al.*, 2003; Creveling *et al.*, 2013). Sometimes, the succession contacts directly with the *Série Negra* Group, without the basal Cambrian clastic units and the contact is an angular unconformity.

Overlapping the Lower Cambrian carbonate succession, a siliciclastic sequence with flysch characteristics is usually recognized (*e.g.* Cumbres alternances, Vila Boim and Lapa Formation; Fig. 2), with metasandstones, metapelites and rare metaconglomerates (Oliveira *et al.*, 1991; Gozalo *et al.*, 2003). Metapelites become significant to the top of sequence. Acritarch and trilobite faunas indicate a Marianian-Biblian age (Lower Cambrian; Delgado, 1905; Oliveira *et al.*, 1991; Gozalo *et al.*, 2003). Interbedded bimodal meta-volcanic rocks with tholeiitic geochemical signature occur in these siliciclastic sequence (*e.g.* Mata and Munhá, 1990; Etxebarria *et al.*, 2006; Sanchez-Garcia *et al.*, 2008; 2010). Over the Marianian-Biblian siliciclastic sequence, a micaceous quartzite package with metric thickness assigned to the Biblian period is described (Quartzite Bar and Castellar Formation; Oliveira, 1984; Oliveira *et al.*, 1991; Liñan *et al.*, 1995; Gozalo *et al.*, 2003; Araújo *et al.*, 2013).

In Middle Cambrian (Fig. 2), the deposition of siliciclastic series (metapelites, metapsammite and metagreywackes) continues, but the bimodal (subaerial and underwater) volcanic component becomes further important (Terrugem Volcano-Sedimentary Complex, Capas de Playón, Umbria-Pipeta Basalts, Los Villares and Alcoches-S. Benito Formation; Oliveira *et al.*, 1991; Sánchez-García *et al.*, 2010; Araújo *et al.*, 2013). The meta-volcanic rocks show an alkaline to alkaline-transitional composition while some felsic terms reveal a peralkaline geochemical affinity (Mata and Munhá 1990; Sanchez-Garcia *et al.*, 2010). The preserved paleontological record (trilobites, brachiopods and Acritarchs) indicates a Middle Cambrian age, ranging from Biblian to Caesarautian (Oliveira *et al.*, 1991; Gozalo *et al.*, 2003; Vera, 2004). Geochronological data in the meta-volcanic rocks are compatible with this temporal window (515-500Ma; Cambrian series 2/3; Sanchez-Garcia *et al.,* 2008; 2010).

To the top of the sequence, as volcanic component gradually decreases, meta-pelites become dominant notwithstanding the sporadic development of thick metagreywacke beds (Fatuquedo and Ossa (?) Formations; Oliveira *et al.*, 1991; Sánchez-García *et al.*, 2010; Araújo *et al.*, 2013). The Fatuquedo Formation is Middle-Upper Cambrian in age, based in acritarch faunas (Mette, 1989). The mafic meta-volcanic rocks contained in the Ossa Formation display alkaline to alkaline transitional features (Mata and Munhá, 1990).

On top of the aforementioned successions an unconformity (paraconformity?) is described, sometimes outlined by a metaconglomerate with decimetre clasts of quartzites, quartz, mafic and felsic magmatic rocks (Oliveira, 1984; Oliveira *et al.*, 1991; Sanchez-Garcia *et al.*, 2010) denoting a sedimentation (or erosional) gap. The absence of the Upper Cambrian sedimentation is a typical feature all over OMZ.

However, in Pedroches, Estremoz and Moura-Ficalho sections (Fig. 2), the Marianian-Biblian unit, or even all the Cambrian clastic units as in Estremoz and Moura-Ficalho, do not appear. In Pedroches section, a sequence of metalimestones (Santo Domingo Formation) of Marianian age with abundant interbedded siliciclastic rocks is described (Gozalo *et al.* 2003; Creveling *et al.*, 2013). In Estremoz and Ficalho-Moura section, over the Lower Cambrian Dolomite Formation, a continuous siliceous horizon is observed, being interpreted as a record of an episode of sub-aerial exposure (Oliveira, 1984; Carvalhosa *et al.*, 1987; Oliveira *et al.*, 1991) that precede the development of volcano-sedimentary complexes with abundant calcite marbles, calc-schists and interlayered bimodal meta-volcanic rocks (Mata and Munhá, 1985; Oliveira *et al.*, 1991; Araújo *et al.*, 2013).

The age of Estremoz and Ficalho-Moura volcano-sedimentary complexes is controversial, with assigned ages ranging from Cambrian to Devonian (Perdigão, 1967; Carvalho *et al.*, 1971; Oliveira, 1984; Carvalhosa *et al.*, 1987; Oliveira *et al.*, 1991). Crinoids fragments and conodonts from Ferrarias marbles (considered by some authors as stratigraphic equivalent to the Estremoz Anticline Marbles; Piçarra, 2000) seems to show an Upper Silurian-Devonian age (Piçarra and Le Menn, 1994; Piçarra, 2000; Sarmiento *et al.*, 2000). Some authors (*e.g.* Lopes, 2003; Pereira *et al.*, 2012a) argue that these ages do not correspond to the depositional age, but the presence of sub-aerial exposure and remobilization of Devonian faunal material. Recently, Pereira *et al.* (2012a) obtained a radiometric age 499.4 ± 3.3 (U-Pb, LA-ICP-MS in zircons) in rhyolites intercalated in the Estremoz marbles, proposing a Guzhangian-Paibian age (Middle-Upper Cambrian). However, the stratigraphic position of the rhyolite sample is uncertain with regard to Estremoz marbles and it is not interbedded in marble sequence (Coelho and Gonçalves, 1970), remaining the age unknown.

II.2.4. Lithostratigraphy of Abrantes region

The work performed in the Abrantes region allows to identify and characterize several lithostratigraphic units (Fig. 3 and 4), which include various rock types distinguishable on the basis of their meso-mircroscopic petrographic features.

The structure of Abrantes region is highly complex due the action of two high-strain deformation episodes (Fig. 3B; Moreira, 2012). The first one (D_1) is poorly preserved and spatially heterogeneous: in axial zone, where the older units outcrops (considered as Neoproterozoic), a low dipping foliation was generated, showing tangential transport to NW. The axial structure is poorly preserved due the action of the second deformation episode (D_2), being well-preserved in Maiorga Granite, Neoproterozoic in age (Mateus *et al.*, 2015). In both limbs of structure,

where outcrops the early units (Paleozoic related), the D_1 folds show opposite geometrical vergence, i.e. to SW in SW limb and to NE in NE limb. The D_1 episode was interpreted as result from a kilometric sheath fold associated to TBCSZ NW termination. The D_2 affects and almost totally transposes all previous structures, being associated with a high-strain dextral non-coaxial deFormation regime, induced by PTFASZ kinematics. The D_2 is characterized by the development of dextral shear zones, with intense strain partition, which rework, reorient, refold and dismember the earliest structure.

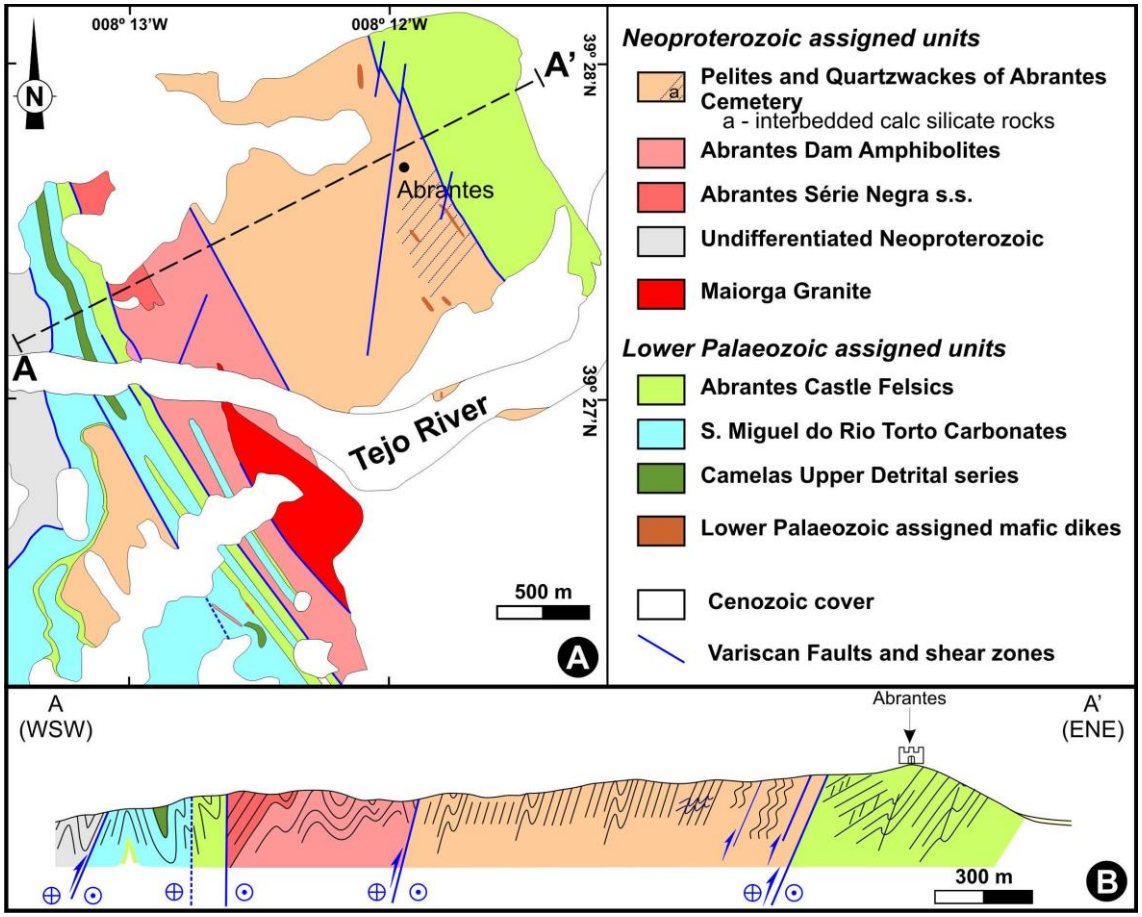

Figure 3 – Simplified geological map of Abrantes (A) and representative cross-section (B), disclosing the spatial relationship between units ascribed to Neoproterozoic and Palaeozoic (map geographic coordinates – WGS 84).

II.2.4.1. Axial zone units – Neoproterozoic related

Three distinct units were recognized in axial zone of Abrantes (Fig. 3), showing strong lithological and petrographic similarities with the Neoproterozoic sections of OMZ (Fig. 2, 4). From the apparent bottom to the top, these units were labelled as: (1) *Abrantes Cemetery Pelites and Quartzwackes,* (2) *Abrantes Dam Amphibolites* and (3) *Abrantes Série Negra s.s.*

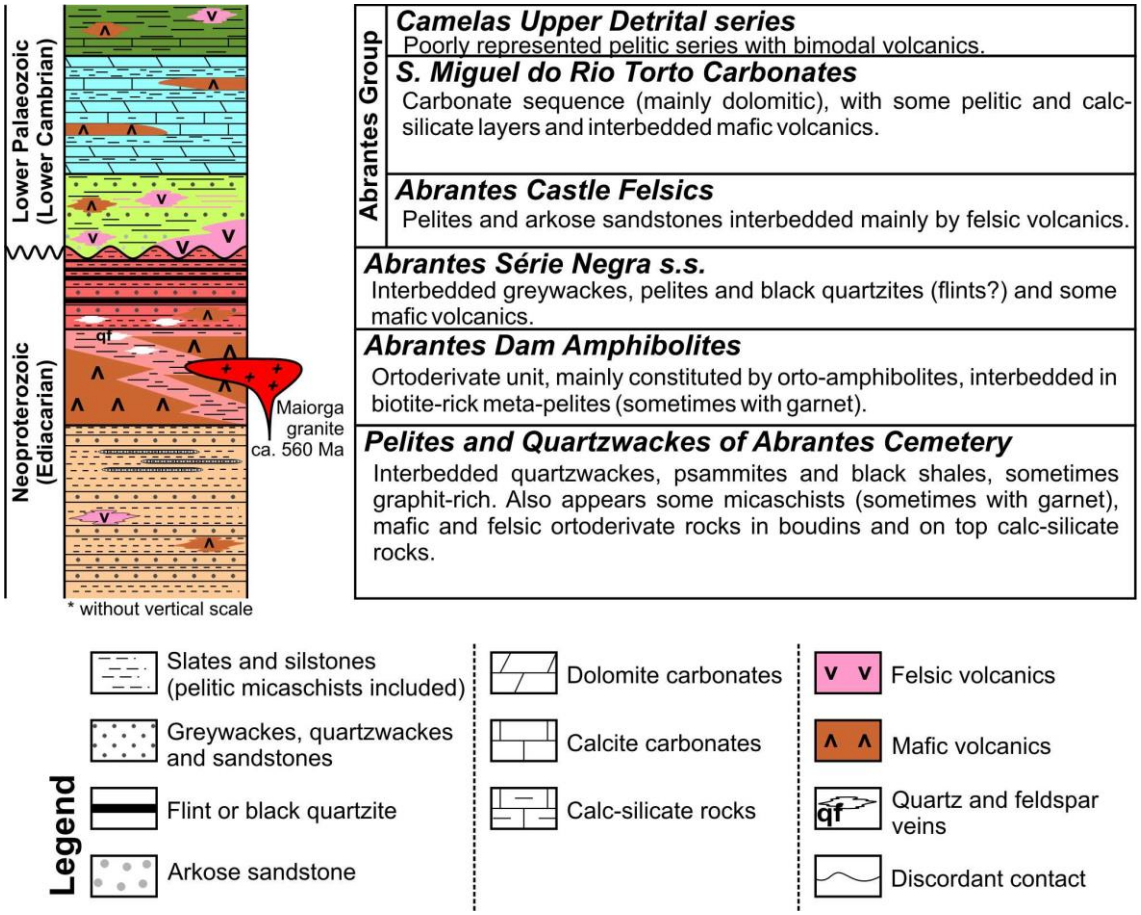

Figure 4 – Lithostratigraphic column proposal for the Abrantes region.

Abrantes Cemetery Pelites and Quartzwackes

This unit is preserved at the eastern sectors of the study area (Fig. 3). The unit is well exposed in Francisco Sá Carneiro Avenue (near Abrantes Cemetery) and in north margin of Tejo River near the Abrantes Dam.

It contacts at East with the Abrantes Castle Felsics (see section 4.2.) and at West with the Abrantes Dam Amphibolites, in both cases through Variscan shear zones. This unit is mostly composed of a siliciclastic succession (Fig. 5A and 5B), which includes decametric thick meta-quartzwackes, metagreywackes, metapsammites, dark phyllites and micaschists (both occasionally hosting thin beds of carbonate beds); heterometric quartz veins preserving evidence of multiphase deformation are present.

Micaschists are usually fine-grained and composed of quartz + biotite ± chlorite ± opaque minerals phases (Fig. 6A), sometimes involving garnet (millimetre-centimetre) porphyroblasts, possibly resulting from Variscan metamorphism blasthesis. To the East, these rocks include intercalations of carbonate beds, sometimes preserving evidences of previous deformation prior

to the Variscan Cycle (Fig. 5C). Similar carbonates also occurs disseminated within phyllites (Fig. 6B), suggesting a silicate protolith with disseminated carbonates. The carbonate features are clearly distinguished from the carbonates assigned to the Lower Palaeozoic (see description below).

In addition, the dark colours displayed by some sections of the metagreywacke/slate succession can be taken as a marker of local enrichments in carbonaceous matter, part of it possibly lately recrystallized as tiny graphite plates (Fig. 6C).

The *Abrantes Cemetery Pelites and Quartzwackes* includes lenses (often boudin-type structures) of felsic and mafic derived rocks (Fig. 5D, 6D and 6E), namely:

- very fine-grained amphibolitic schist (Fig. 6D; sample GQAB 20), with mafic nature, whose grano-nematoblastic matrix comprises strips enriched in preferentially oriented green (to bluish) amphibole interspersed with bands composed of plagioclase, quartz, muscovite and opaque mineral phases; garnet and plagioclase porphyroblasts reaching centimetre dimensions (1-2 cm; Fig. 5D) and commonly rimmed by late chlorite.
- fine-grained meta-volcanic felsic rock (Fig. 6E; sample GQAB 18) with nodular texture, presenting abundant garnet (sometimes elliptical in shape) and prismatic andalusite porphyroblasts. The matrix includes quartz + feldspar + biotite + opaque mineral phases ± muscovite. Garnet is millimetric in size and associated with green amphibole; late developed rims of biotite and chlorite outline the metamorphic retrogression path.

Abrantes Dam Amphibolites

The best unit cross-section is in the southern bank of Tejo River, near Abrantes Dam. The Abrantes Dam Amphibolites represents a volcano-sedimentary sequence, mostly composed of mafic ortho-derived rocks (Fig. 5E), being interbedded with a minor siliciclastic component (Fig. 4 and 5F).

Abundant quartz ribbons with millimetre to centimetric thick are usual; quartz display evidence of significant dynamic recrystallization leading to polygonal arrangements that preserve grains with wavy-undulatory extinction. Centimetre to decimetre lenses of quartz-feldspathic rocks can be occasionally recognized.

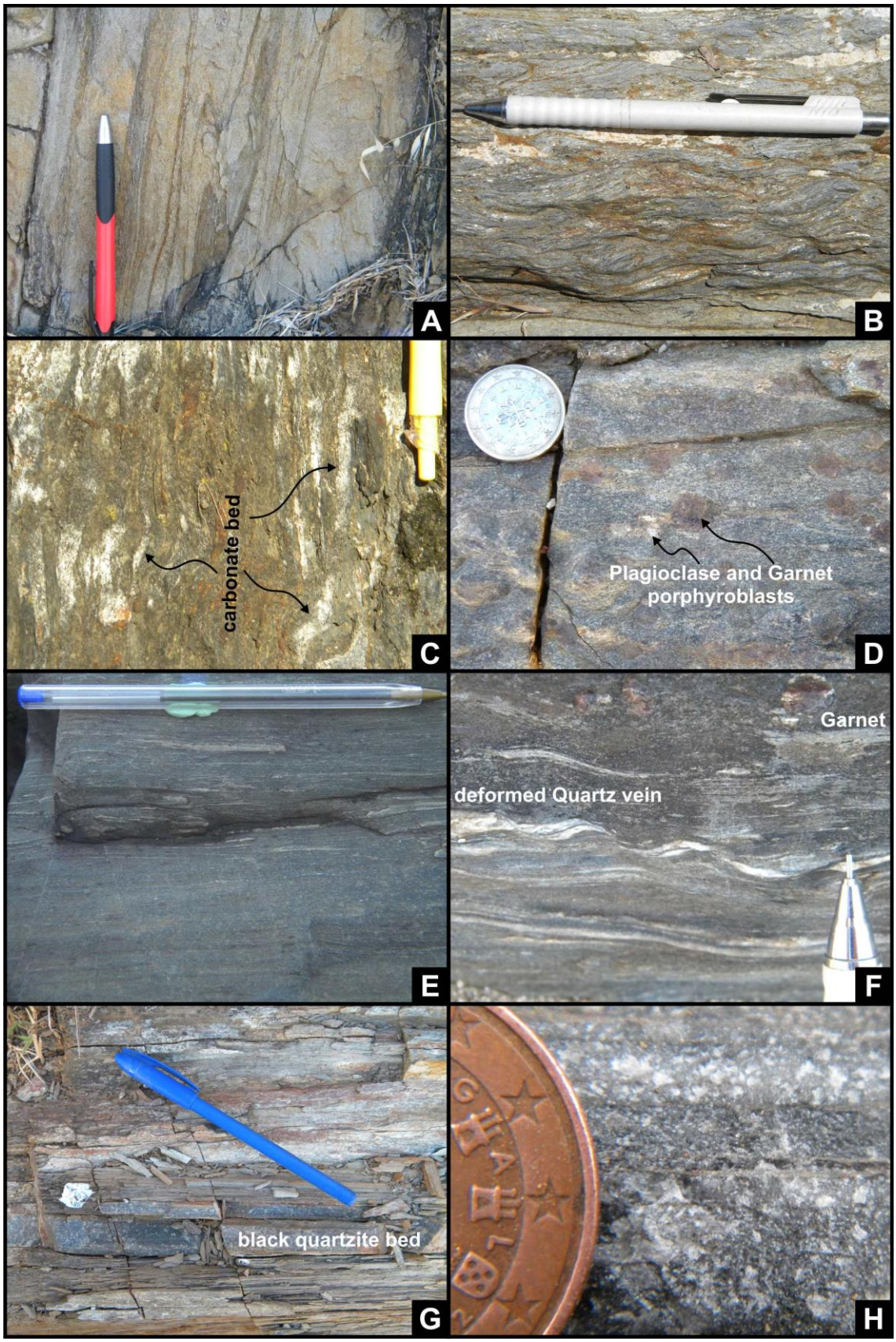
A
B
carbonate bed
C
Plagioclase and Garnet
porphyroblasts
D
E
Garnet
deformed Quartz vein
F
black quartzite bed
G
H

Figure 5 – Macroscopic features displayed by rocks types forming the Neoproterozoic assigned units:

Pellites and Quartzwackes of Abrantes Cemetery

A – Typical showing of meta-(quartz)greywacke and metapellite sequence.

B – Sheared micaschist.

C – Typical showing of micaschist interbedded with calcite metalimestone beds.

D – Typical showing of mafic/intermediate ortho-derived rock (amphibole schist), preserved in a boudin-type structure developed within siliciclastic series – Sample GQAB 20.

Abrantes Dam Amphibolites

E – Representative specimen of amphibolite – Similar to samples GQAB 5A and 5B.

F – Distinctive biotite-rich metapellite with garnet and deformed quartz veins.

Abrantes Série Negra s.s.

G – Interbedded black quartzites in black metapelites (here, the characteristic black colour is partially modified by chemical weathering).

H – Textural detail of a recrystallized black quartzite.

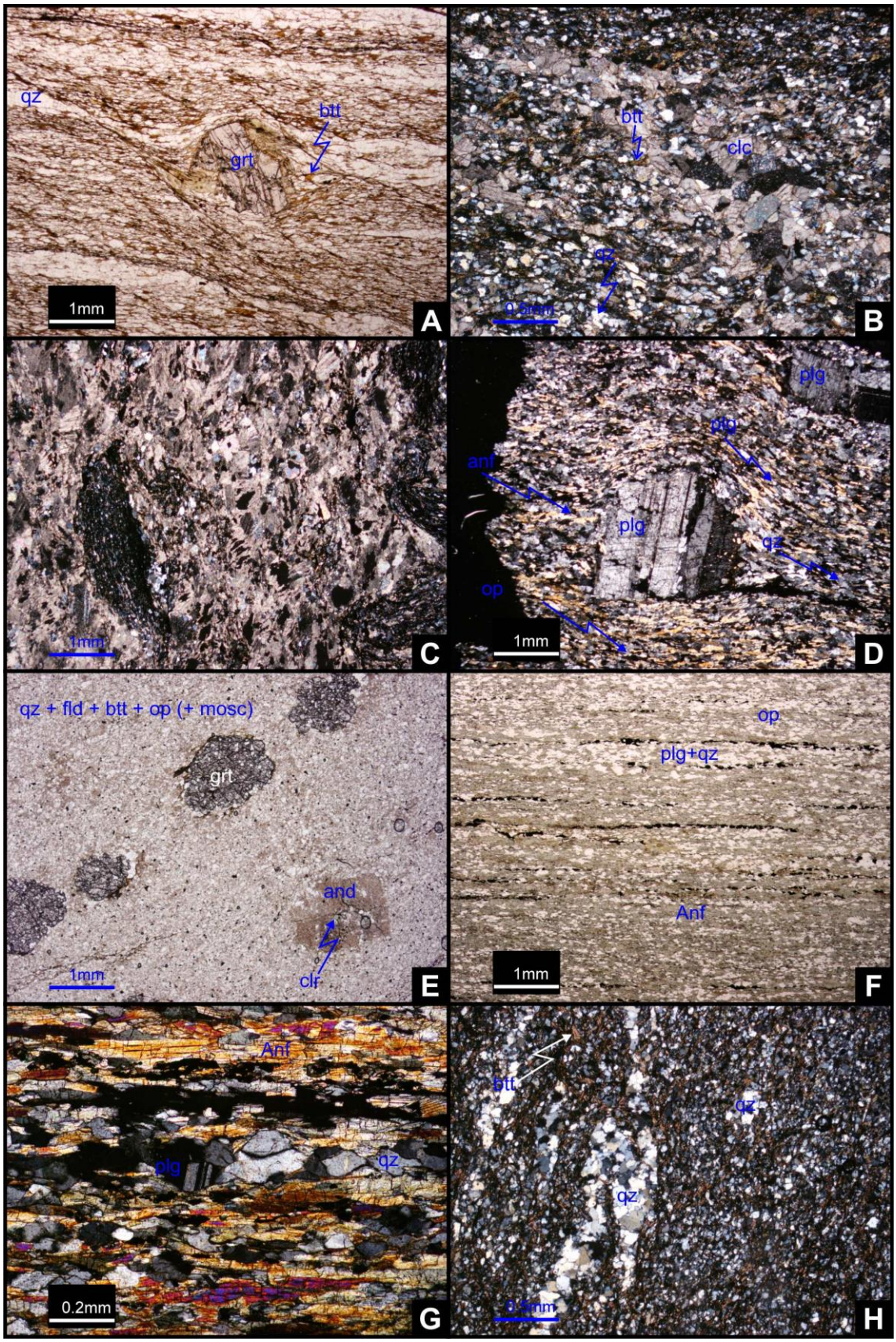
qz
btt
grt
1mm
A
btt
clc
qz
0.5mm
B
1mm
C
plg
plg
anf
plg
qz
op
1mm
D
qz + fld + btt + op (+ mosc)
grt
and
cl
1mm
E
op
plg+qz
Anf
1mm
F
Anf
plg
qz
0.2mm
G
btt
qz
qz
0.5mm
H

Figure 6 – Microscopic features displayed by rocks types forming the Neoproterozoic assigned units (mineral abbreviations according to Whitney and Evans, 2010: grt – garnet; qz – quartz; bt – biotite; cal – calcite; amp – amphibole; op – opaque minerals; pl – plagioclase; fsp – undifferentiated feldspar; ms – muscovite; and – andaluzite; chl – chlorite; zrn – zircon; dol – dolomite; gr – graphite; ep – epidote):

Pellites and Quartzwackes of Abrantes Cemetery

A – Fine-grained biotite-rich micaschist with garnet porphiroblast (parallel nicols).

B – Common carbonate matrix of micaschist, showing calcite grains dispersed in silicate minerals (crossed nicols).

C – Calcite-rich cataclastic rock, including fragments of a previous deformed graphite-rich metapelites (crossed nicols).

D – Plagioclase porphiroblast in a quatz-feldspar-amphibole matrix of a mafic ortho-derived rock (amphibole schists) interspersed in siliciclastic series as boudin-type structures (crossed nicols) – Sample GQAB 20.

E – Textural and mineralogical features of fine-grained felsic ortho-derived rock interspersed in siliciclastic series as boudin-type structure (parallel nicols) – Sample GQAB 18.

Abrantes Dam Amphibolites

F – Fine-grained oriented nematoblastic texture, showing interleaves of amphibole rich and quartz-plagioclase rich bands (parallel nicols) – Sample GQAB 5A.

G – Textural detail of a representative amphibolite (crossed nicols) – Sample GQAB 5A.

H – Fine-grained biotite-rich pelitic schist, representative of metapelites which forming this unit, showing also a deformed quartz vein (crossed nicols).

The amphibolites (Fig. 6F and 6G) comprise medium to fine-grained green amphibole + plagioclase + quartz + opaque minerals phases ± feldspar (± fine-grained, secondary muscovite related with feldspar alteration; samples GQAB 5A and 5B). The texture is strongly oriented, nematoblastic to granonematoblastic, with the development of amphibole (± opaque mineral phases) bands alternating with quartz + feldspar s.l. ones. The intense S-L fabric presented in these amphibolites and its medium to fine-grained texture seems to show the mylonitic processes associated to metamorphism. The metamorphic mineralogical assemblage, under amphibolite facies metamorphism, seems to show a mafic origin to these ortho-derived rocks. The primary texture was totally obliterates.

The siliciclastic component is represented by fine-grained biotite-rich black phyllites/schists, essentially comprising quartz + biotite ± opaque minerals phases ± undifferentiated feldspar ± garnet (Fig. 6H). It is also possible to highlight the presence of deformed quartz ribbons, exhibiting granolepidoblastic texture, polygonal textures and wavy-undulatory extinction.

Abrantes Série Negra

The Abrantes *Série Negra* ("*Black Series*") contact the Abrantes Dam Amphibolites in stratigraphic continuity. This succession are poorly outcropping and the best section to see its lithostratigraphic features is on hillside at south of Abrantes Municipal Pool Complex, in north margin of Tejo River.

The former unit includes a siliciclastic succession mainly composed of metagreywackes, metapsammites, metapellites and black slates (some of them graphite-rich); occasionally interlayered bimodal meta-volcanics can be seen.

Within this siliciclastic succession with black colours, it was recognized millimetre to centimetre thick black quartzites (or flints?; Fig. 5G and 5H). This lithotype and the low abundance of amphibolites were used as distinguish criteria between this unit and the Abrantes Dam Amphibolite Unit, which do not contain black quartzites.

4.2. Abrantes Group – Paleozoic related units

The Abrantes Group expression was firstly used by Conde (1984), although, not providing its comprehensive characterization. The same label is here reused to encompass the volcano-sedimentary units with Paleozoic litostratigraphic affinities.

Abrantes Castle Felsics

The unit cropping out in East and West of study area and it contacts with the Neoproterozoic related units through shear zones, being its stratigraphic positioning complex. The best cross-sections for this unit are, to the East, in Francisco Sá Carneiro Avenue and in northern bank of Tejo River, at West section.

This succession comprises a meta-volcano-sedimentary sequence where siliciclastic layers (psammites, pelites and arkoses), with bright colours, enclose volcanic-derived levels with rhyodacitic nature (Fig. 7); syn-metamorphic centimetre quartz veins are common. At NE, near Barca do Pego (Fig. 1B), the sequence also includes metaconglomerates.

In the eastern section of the study area (Fig. 3) the unit thickness is higher than at west and the volcanic component is more significant, locally preserving features compatible with a volcaniclastic origin (Fig. 7B; samples GQAB 17 and 28), as primary layering. The prevalent quartz-feldspar mineral assemblage is complemented by large amounts of chlorite + epidote + biotite + opaque mineral phases (mainly pyrite; Fig. 7B to 7D), which compose the thin-grained matrix. The systematic presence of preferentially oriented biotite and chlorite (+ epidote) in rock matrix indicates progression of metamorphic recrystallization under greenschist facies conditions (transitional of chlorite-biotite zones), somewhat below those achieved in axial sectors (amphibolite-greenshist transitional facies). Epidote occurs as disseminated grains within the fine-grained matrix, as well in late narrow bands/veins together with non-deformed chlorite and pyrite, cutting across early structures, possibly reflecting the retrogression path evolution or hydrothermal processes (Fig. 7C, 7D).

In the western section, the rhyodacites display an evident granoblastic equigranular texture, usually with submillimetre dimensions, and comprise abundant quartz and feldspar (along with plagioclase; Fig. 7E; sample GQAB 26), besides accessory amounts of biotite + fine-grained muscovite + zircon + opaque mineral phases (Fig. 7E). Some of these bodies are stratified, with intense dynamic recrystallization, possibly related with the Variscan metamorphic event. Locally, some amphibolite dykes are also identified (sample AB 41).

In addition, a decametric sub-volcanic rhyodacite body occurs within this unit. This body presents fine-grained equigranular mosaic texture, being composed of abundant quartz + feldspar + plagioclase, occasionally with biotite + amphibole ± muscovite (Fig. 7F).

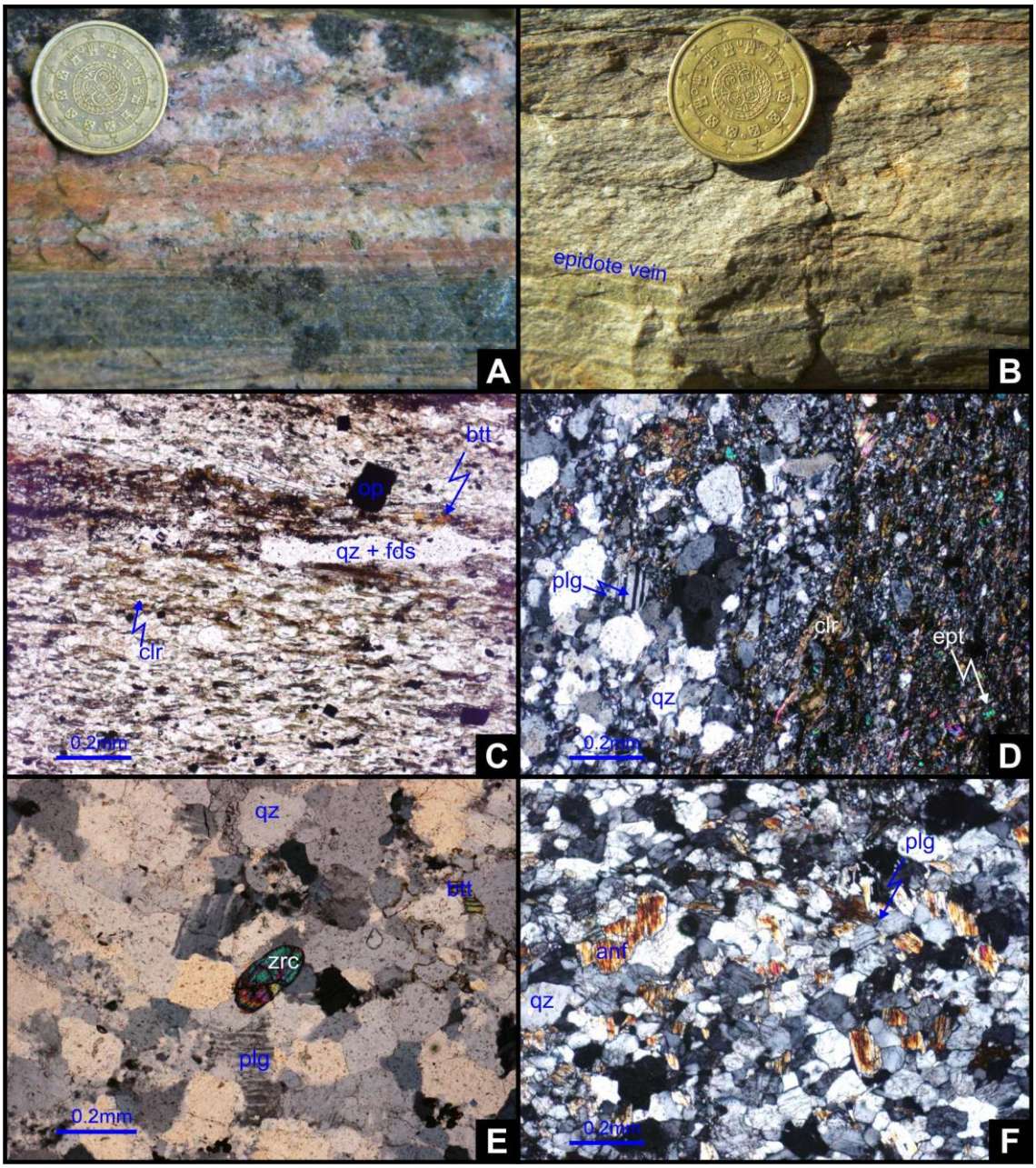
A
epidote vein
B
btt
op
qz + fds
clr
0.2mm
C
plg
clr
ept
qz
0.2mm
D
qz
btt
zrc
plg
0.2mm
E
plg
ant
qz
0.2mm
F

Figure 7 – Macro and microscopic features of Abrantes Castel Felsics (Abrantes Group – assigned to Lower Palaeozoic; mineral abbreviations as in Fig. 6):

A – Felsic banded rock cropping out at the western sector of the study area.

B – Meta-volcanic stratified rock representative of east section of the study area; note the development of epidote-bearing veins sub parallel to the primary planar structure.

C – Eastern sector meta-volcanic stratified rock, displaying late disturbance of the early oriented texture by opaque cubic minerals (pyrite), formed during the retrogression path (parallel nicols).

D – Epidote-chlorite late-developed vein cutting the meta-volcanoclastic rock in eastern sector of the study area (crossed nicols).

E – Textural and mineralogical features of a rhyo-dacite recrystallized body interbedded in volcaniclastic series (crossed nicols) – Sample GQAB 26.

F – Decametric rhyo-dacite body preserved in the eastern sector of the study area (crossed nicols).

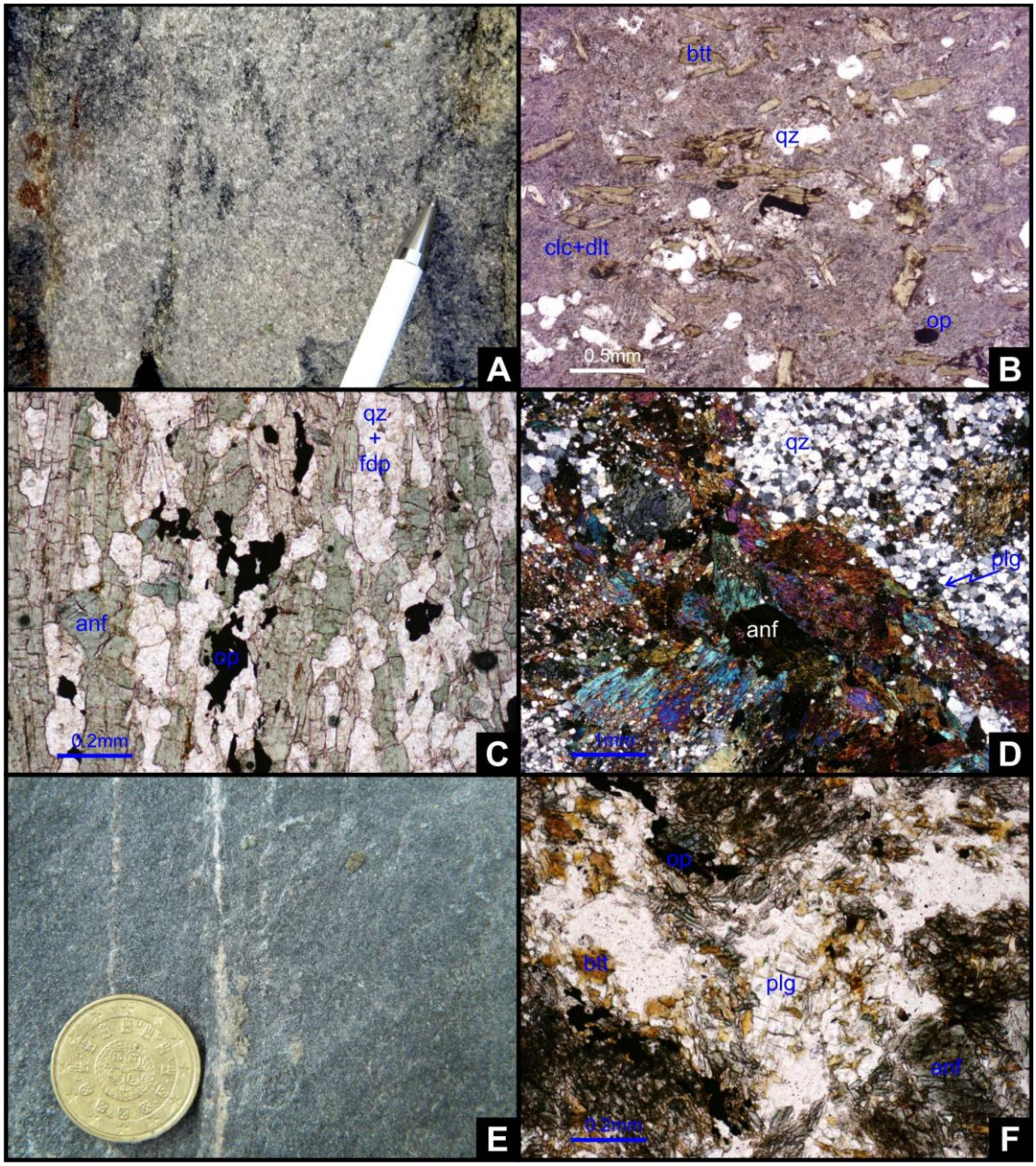
A
btt
qz
clc+dlt
op
0.5mm
B
qz
+
fdp
anf
op
0.2mm
C
qz
plg
anf
1mm
D
E
op
btt
plg
anf
0.2mm
F

Figure 8 – Macro and microscopic features of the S. Miguel do Rio Torto Carbonates and the Camelas Upper Detrital series (Abrantes Group – assigned to Lower Palaeozoic; mineral abbreviations as in Fig. 6):

A – Dolomite-rich marbles representative of the S. Miguel do Rio Torto Carbonates.

B – Typical silicate minerals (quartz and biotite) in a carbonate (calcite and dolomite) matrix (parallel nicols).

C – Nematoblastic texture of green amphibole arrays forming the mafic/intermediate ortho-derived rocks observed in the Camelas Upper Detrital series (parallel nicols) – Sample AB 46.

D – Main mineralogical constituents of mafic/intermediate ortho-derived rocks observed in the Camelas Upper Detrital series; note the evident quartz polygonal texture (crossed nicols).

E – Representtie ortho-derived fine-grained textured grey-greenish body interlayered in the S. Miguel do Rio Torto Carbonates.

F – Mafic dyke with coarse-grained texture attributed to Lower Palaeozoic, cutting the Neoproterozoic assigned units. The magmatic mineral assemblage and textures are completely obliterated by Variscan metamorphic products (crossed nicols) – Sample GQAB 14.

S. Miguel do Rio Torto Carbonates

Overlying the Abrantes Castle Felsics, a (siliciclastic-)carbonate unit is developed, being its transition gradual. The unit comprises dominant dolomite-rich marbles (Fig. 8A) with intercalations of calcite marbles and, ocassionally, calc-schists and metapelites. Evidences of secondary late dolomitization can be observed (Moreira *et al.* 2016). Usually these marbles displays pink to whitish colours but the relative abundance of disseminated epidote within the carbonate matrix may generate greenish marbles.

Carbonate rocks include a significant siliciclastic component (Fig. 8B) mainly composed of quartz (grain sizes up to centimetre) + feldspar *s.l.* + micas (biotite > muscovite); occasionally opaque mineral phases are also recognised. The abundant siliciclastic component is interpreted as a result of a proximal (continental) source. Calc-shist rocks (quartz + mica > carbonates) interbedded with marbles are scarce and display grey colours. They may represent either (felsic) volcanic-derived products highly modified by metasomatic process, or sedimentary-derived (marly limestones) products.

Commonly, black-greenish rocks within the siliciclastic sequence (Fig. 8E) are observed, forming sill-like or boudin-like bodies interpreted as (mafic) meta-volcanic-derived products synchronous of carbonate sedimentation (samples AB 40, AB 48, AB 77-A, GQAB 19). These rocks display fine-grained grano-nematoblastic texture and comprise plagioclase + amphibole + biotite + opaque mineral phases ± chlorite ± quartz ± titanite. Similar bodies intrude the Neoproterozoic assigned sequence of Abrantes Cemetery Pelites and Quartzwackes unit (sample GQAB 14), possibly representing dykes feeding the volcanic products included in the Palaeozoic assigned units. Their textures are coarse-grained and the mineral assemblage is consistent with a dolerite protolith (Fig. 8F).

Camelas Upper Detrital series

The sequence assigned to the Early Palaeozoic culminates with a late and poorly represented volcano-siliciclastic succession, occupying synfom cores (Fig. 3). The transition between this unit and the S. Miguel do Rio Torto Carbonates appears to be gradual; the basal succession also includes carbonate-rich layers that fade towards the succession's top.

The siliciclastic components prevail over those volcano-derived and comprise fine-grained rocks, namely dark-grey to black phyllites. The amphibolites display strongly oriented nematoblastic (due to amphibole grains stretching) to grano-nematoblastic (evident polygonal/mosaic of plagioclase/feldspar±quartz) textures and are composed of green to

brownish prismatic amphibole + plagioclase + opaque mineral phases + feldspar ± quartz (Fig. 8C and 8D), suggesting a mafic volcanic protolith (samples AB 46 and GQAB 25).

II.2.4.3. Geochemical data of (meta)volcanic lithotypes

In this study, for the litostratigraphic correlation between Abrantes region and the other OMZ litostratigraphic sequences, 16 samples from Abrantes were selected for whole-rock geochemical analyses: (1) two felsic rocks and two amphibolite from the Abrantes Cemetery Pelites and Quartzwackes Unit (one is considered a Cambrian dyke as previously mentioned), (2) two amphibolites from the Abrantes Dam Amphibolites Unit; (3) three felsic rocks and one amphibolite from Abrantes Castle Felsics Unit; (4) four amphibolites interbedded in S. Miguel do Rio Torto Carbonates Unit; and, finally, (5) two amphibolites from the Camelas Upper Detrital series. Join to these samples, seven samples from Alter-do-Chão-Elvas sector, near Vila Boim village, are also collected: (1) two felsic rocks from basal Cambrian Unit, (2) 4 mafic to intermediate meta-volcanic rocks interbedded in Elvas Carbonated Formation and (1) one mafic rock from Vila Boim Formation. The Vila Boim volcanic rocks was selected because in this sector the Cambrian stratigraphy was well constrained by several studies (Oliveira *et al.*, 1991; Gozalo *et al.*, 2003; Moreira *et al.*, 2014b) and it is possible to compare the geochemical fingerprint of interbedded volcanic rocks, allowing a stronger correlation.

Major and trace elements were analyzed at the Activation Laboratories - ACTLABS (Canada) using the lithium metaborate/tetraborate fusion for ICP (WRA Code 4B) and ICP-MS (WRA Code 4B2). Samples were fused with a flux of lithium metaborate and lithium tetraborate in an induction furnace. The melt mixed with 5% nitric acid containing an internal standard until completely dissolved. The samples were run for major and trace elements on a combination of simultaneous/sequential Thermo Jarrell-Ash ENVIRO II ICP. Calibration was performed using seven USGS and Canmet certified reference materials. One of the seven standards is used during the analysis for every group of samples. The sample solution prepared under Code 4B is spiked with internal standards to cover the entire mass range, is further diluted and is introduced into a Perkin Elmer Sciex ELAN 6000, 6100 or 9000 ICP-MS using a proprietary (ACTLABS) sample introduction methodology. Analytical precision and accuracy for major elements are 1 to 2% and better than 5% for trace elements. Whole-rock geochemical data and analytical methods are summarized in Table I (Abrantes) and II (Vila Boim).

II.2.4.3.1. Abrantes magmatic rocks

Besides the variation in LOI contents (Loss on Ignition; 0,43-5,31%), major element compositions and Alkalis (Na_2O+K_2O) contents vs SiO_2 (Le Maitre *et al.*, 1989; Fig. 9A1) recognize the previous subdivision in felsic and mafic rocks. The felsic rocks (two metadacites and three metarhyolites; Le Maitre *et al.*, 1989) display high contents in SIO_2 (65,54-81,50%) and lower in TiO_2 (0,25-0,71%), $Fe_2O_{3(tot)}$ (0,88-6,93%) and MgO (0,10-2,19%), while the mafic rocks (amphibolites corresponding to basalts and one trachy-basalt; Le Maitre *et al.*, 1989) display SiO_2 values lower than 51% (45,99-50,85%) and higher values in TiO_2 (1,73-3,85%), $Fe_2O_{3(tot)}$ (9,98-16,11%) and MgO (3,67-9,71%) when compared to the felsic rocks. The Al_2O_3 is homogeneous (13,38-16,11%) in mafic rocks and more variable in felsic ones (9,85-16,66%).

The data show that the felsic rocks are subalkaline with homogenous Alkalis content (5,55-6,40%; Fig. 9A1) and the projection in AFM diagram (Fig. 9A2) shows a dispersion between the tholeiitic and calk-alkaline series. Mafic rocks are plotted on alkaline and subalkaline fields with Alkalis ranging from 2,78 to 6,84% (Fig. 9A1). The data projection from mafic rocks in the AFM diagram (Fig. 9A2) shows a tholeiitic features for all samples, being projected near the Irvine and Baragar (1971) curve, exception for sample AB 46 projected in calk-alkaline series field duo to the high Alkalis content, although very closed from the curve, being an exception.

The metadacites with SiO_2 ranging between 66,08 and 67,00% and Alkalis between 5,60-6,40% are distinguish from the three metarhyolites with high silica content (77,18-81,93%) and persistent Alkalis percentage (5,55-5,72%). The metarhyolite GQAB 26 presents higher content in Na_2O (5,65%) and lower K_2O (0,07%), while the two metarhyolites (GQAB 17 and GQAB 28) presents similar contents in K_2O and Na_2O (2,20-3,23% and 2,32-3,39%, respectively).

The metadacites with Alumina Saturation Index (ASI; Frost *et al.* 2001) between 3,47 and 3,88 (Fig. 9B) are peraluminous (GQAB 16 is a ferroan-dacite and sample GQAB 18 is a magnessian-dacite). The metarhyolites have considerable contents in Al_2O_3 (9,9-11,0%) and its ASI are also consistent with peraluminous nature (1,79-2,86; Fig. 9B), although lower than the determinate in metadacites. Nevertheless, the sample GQAB 26 is more magnesian (MgO 0,93%), whereas the other two (GQAB 17 and GQAB 28) are ferriferous ($Fe_2O_{3(tot)}$ 1,8-3,2%; Fig. 9B).

As mentioned, the mafic rocks are amphibolites, corresponding to ten basalts and one trachy-basalt (GQAB 19). The amphibolites (metabasalts) present typical major elements values for mafic rocks (Al_2O_2 13,44-16,24%; K_2O 0,24-1,14%; Na_2O 2,19-4,32%; CaO 7,45-10,66%). The $Fe_2O_{3(tot)}$ (10,51-16,24%) and MgO (3,70-10,22%) values vary significantly. The samples GQAB 5B and GQAB 20 present lower contents in MgO (4,88 and 3,70% respectively) and higher $Fe_2O_{3(tot)}$

contents (14,61 and 16,24% respectively), while in the other samples the MgO (5,88-10,22%) and $Fe_2O_{3(tot)}$ contents (10,51-13,66%) are quite homogeneous. Consequently, the GQAB 5B and GQAB 20 samples presents lower #Mg (23,00-30,47) compared with the other ones (36,97-56,06). The TiO_2 content also shows this separation with higher values in GQAB 5B and GQAB 20 (3,53-3,86%) and lower ones in other samples (1,76-2,92%). Finally, the outlier amphibolite GQAB 19 (metatrachy-basalt) is distinguish from the other amphibolites because have high values of K_2O (3,10%), lower CaO content (5,09%) and in the #Mg (27,29), which reflect the higher content in $Fe_2O_{3(tot)}$ (15,96%) relatively to MgO (4,57%).

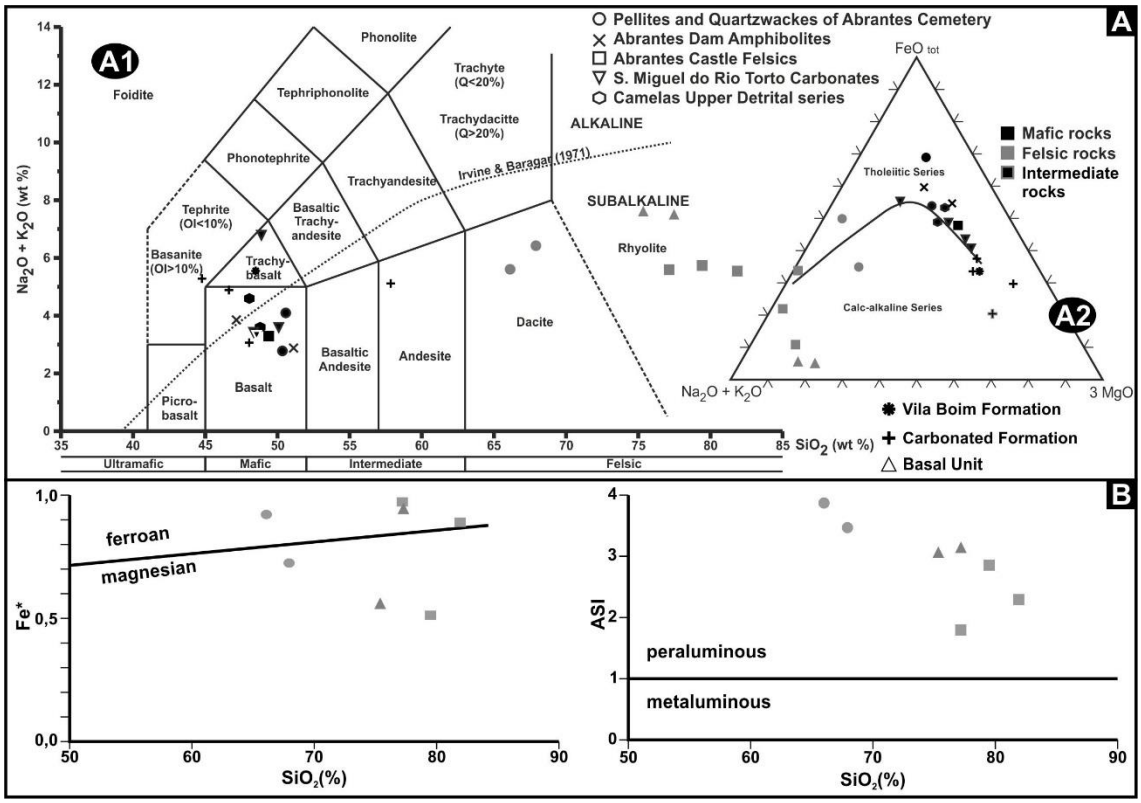

Figure 9 – Geochemical features of analysed volcanic derived rock from Abrantes and Vila Boim:

A – Total Alkalis vs. Silica diagram (A1; adapted from Le Maitre *et al.*, 1989) and AFM diagram (A2; adapted from Irvine and Baragar, 1971)

B – Fe* and ASI vs Silica diagrams applied to felsic rocks (adapted from Frost *et al.*, 2001).

Due to metamorphism and/or weathering processes the variations in the HFSE (High Field Strength Elements) like REE, Th, Nb, Ta, Zr, Hf, Ti, Y, etc. seem more reliable indicators of the igneous petrogenesis (e.g. Pearce, 1982; Rollinson, 1993), and should reflect the primary igneous features. Therefore, the geochemical data analysis and the subsequent petrogenetic interpretation will be based in the trace element geochemical variations and according with litostratigraphic correlation of units which they are sampled.

Rocks from Neoproterozoic assigned Litostratigraphic Units

This sample group includes: (1) two metadacites (GQAB16 and GQAB 18) and one amphibolite (GQAB 20) from the Abrantes Cemetery Pelites and Quartzwackes Unit and (2) two amphibolites from the Abrantes Dam Amphibolites Unit (GQAB 5A and GQAB 5B). The amphibolite interpreted as a Cambrian metadolerite dyke sampled in Abrantes Cemetery Pelites and Quartzwackes Unit will be analysed joint to the samples from Cambrian related litostratigraphic units.

The REE contents plotted in a normalized primitive mantle diagram (Fig. 10A) shows similar patterns for metadacites, nevertheless the sample GQAB18 is somewhat enriched in REE contents. Both samples present negative Eu anomalies (Eu/Eu* 0,67-0,78) and are enriched in LREE relatively to MREE and HREE ($[La/Sm]_n$ = 3,49 to 2,83; $[La/Yb]_n$ = 8,06 to 5,33). The normalized ratios between LREE and HFSE, like Nb and Th, shows a slightly to moderate enrichment in La relative to Nb ($[La/Nb]_n$ = 1,05 to 2,51) and depleted La relative to Th ($[La/Th]_n$ = 0,32 to 0,83; Fig. 10B).

The more enriched feature of sample GQAB 18, relatively to GQAB 16 (Fig. 10B), revelled by REE contents is also present in other incompatible elements like Nb, Ta, La, Sm, Zr, Tb, Y, Tm and Yb. However, Ti have lower values in GQAB 18 (3209 ppm) than in GQAB 16 (4275 ppm) and Th presents similar values (10,95±0,35ppm).

The sample GQAB 16 presents higher Th/Ta ratios (11,2), while sample GQAB 18 have lower ratio value (2,1), attributing an orogenic affinity to GQAB 16 and anorogenic features to GQAB 18 (Fig. 11A; Gordon and Schandl, 2000). A similar behaviour is also revealed by Nb-Y and Ta-Yb diagrams (Fig. 11B; Pearce *et al.*, 1984), suggesting that the ferroan-dacite (GQAB 16) can be related with orogenic magmatism, whereas the magnessian-dacite (GQAB 18) show affinities with within-plate magmatism.

The three amphibolites display variable values in REE. The REE and HSFE normalized primitive mantle plots (Fig. 10A and 10B) define two distinct patterns:

(1) Amphibolite GQAB 5A: the sample is depleted in LREE relatively to MREE and HREE ($[La/Sm]_n$ = 0,50; $[La/Yb]_n$ = 0,51), with enrichment in La relative to Nb and Th ($[La/Nb]_n$ = 2,16; $[La/Th]_n$ = 3,17) and show affinities with the HFSE patterns presented by N-MORB (Sun *et al.*, 1979; Sun and McDonough, 1989).

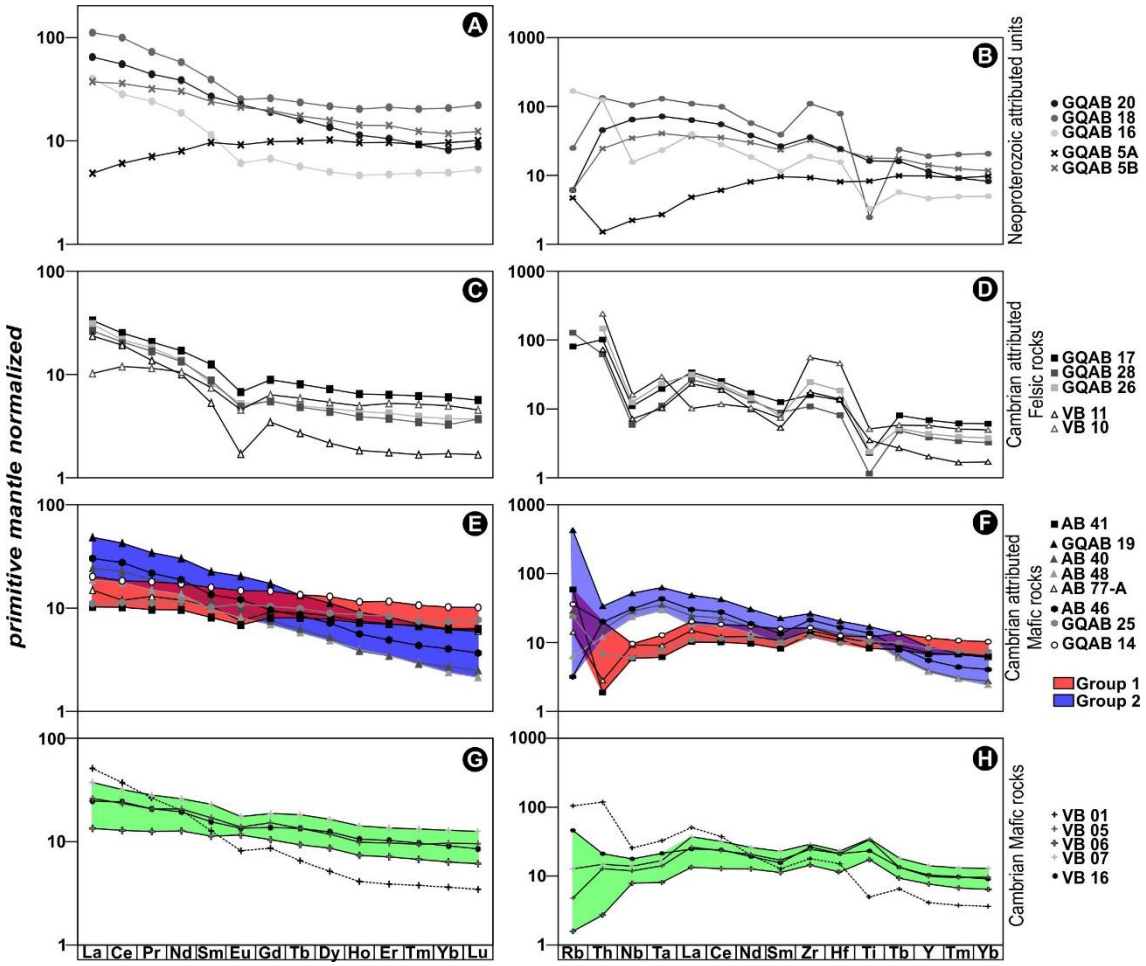

Figure 10 – Primitive mantle-normalized REE and HFSE diagrams (primitive mantle values according to Sun and McDonough, 1989).

(2) Amphibolites GQAB 5B and GQAB 20: these samples are enriched in LREE with respect to MREE and HREE ($[La/Sm]_n$ = 1,55 to 2,40; $[La/Yb]_n$ = 3,17 to 7,87). The LREE shows similar content relatively to Nb and Th ($[La/Nb]_n$ = 0,99 to 1,06; $[La/Th]_n$ = 1,42 to 1,51). However, despite the general highest values in REE in GQAB 20 sample the similar REE and HFSE patterns between these two samples, shows similarities with anorogenic basalts such as OIB and E-MORB (Sun *et al.*, 1979; Sun and McDonough, 1989).

These amphibolites do not present anomalies in Eu ([Eu/Eu*] 0,94 to 0,97). Amphibolite GQAB 5A presents [Zr/Y] = 2,3, and [Hf/Ta] = 22,7, while amphibolites GQAB 5B and GQAB 20 have higher values of [Zr/Y] (5,8 to 7,7) and lower [Hf/Ta] (2,5 to 4,4). The variations in HFSE ratios and data plot in Zr/Y vs Zr (Fig. 12A; Pearce and Gale, 1977; Pearce, 1982; 1983), Th/Yb vs Ta/Yb (Fig. 12B; Pearce, 1982) and Hf-Th-Ta (Fig. 12C; Wood, 1980) diagrams are in agreement with the REE patterns and suggest anorogenic tholeiitic fingerprints such as N-MORB (GQAB 5A) to within-plate tholeiitic to alkali-tholeiitic basalts (GQAB 5B and GQAB 20).

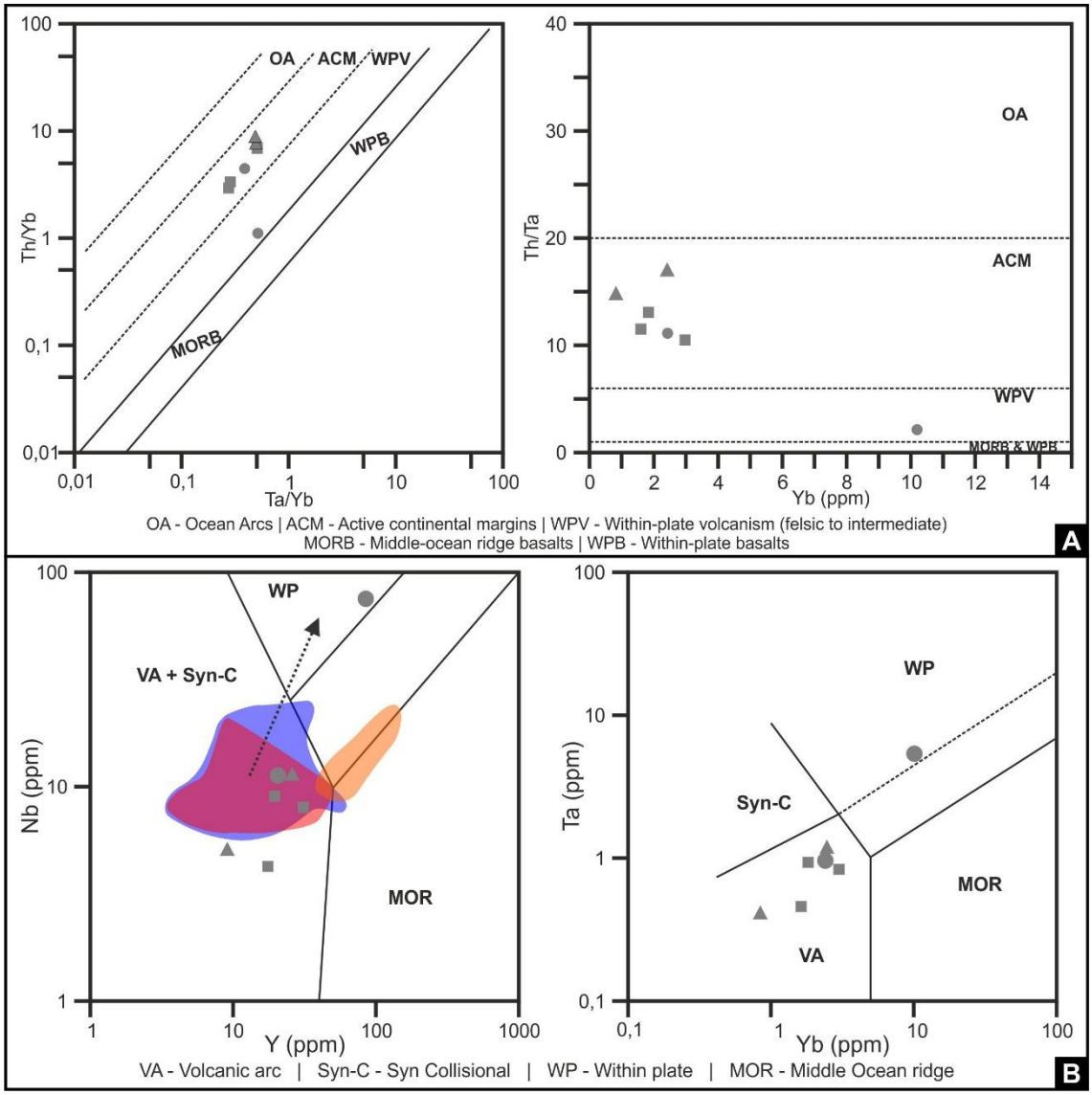

Figure 11 – Discriminant diagrams for the felsic derived volcanic rocks:

A – Th, Ta and Yb relations diagrams (adapted from Gordon and Schandl, 2000);

B – Nb vs Y and Ta vs Yb diagrams (adapted from Pearce *et al.*, 1984).

Rocks from Cambrian assigned Litostratigraphic Units

This sample group is composed of eleven samples: (1) one amphibolite (GQAB 14) considered a Cambrian dyke from the Abrantes Cemetery Pelites and Quartzwackes Unit, (2) three metarhyolites (GQAB 17, GQAB 26, GQAB 28) and one amphibolite (AB 41) from Abrantes Castle Felsics Unit; (3) four amphibolites (GQAB 19, AB 40, AB48, AB 77-A) interbedded in S. Miguel do Rio Torto Carbonates Unit; and (4) two amphibolites (GQAB 25, AB 46) from the Camelas Upper Detrital series.

The REE contents of metarhyolites, plotted in a normalized primitive mantle diagram (Fig. 10C), display patterns with negative anomalies in Eu (Eu/Eu* = 0,63-0,76), being enriched in LREE with respect to MREE and HREE ($[La/Sm]_n$ = 2,66 to 3,74; $[La/Yb]_n$ = 5,53 to 8,23). The LREE are enriched relatively to Nb ($[La/Nb]_n$ = 2,46 to 4,47) and depleted relative to Th ($[La/Th]_n$ = 0,21 to 0,42). The HFSE normalized primitive mantle diagram (Fig. 10D) display similar patterns for the three metarhyolite samples with enrichments in the more incompatible HFSE (i.e. Th, Ta, La) relatively to the less incompatible HFSE (i.e. Tb, Y, Tm, Yb) coupled with negative Ti and Nb anomalies.

The metarhyolites show a Th/Ta ratio range between 10,5 and 13,1, which are common in active continental margins (Fig. 11A; Gordon and Schandl, 2000). The same geochemical feature are assigned by Nb-Y and Ta-Yb discriminant diagrams (Fig. 11B; Pearce *et al.*, 1984), being projected in volcanic-arc volcanism field.

The amphibolites (metabasalts and metatrachy-basalt) data plot in a primitive mantle normalized REE and HSFE diagrams (Fig. 10E and 10F) display two distinct patterns:

(1) Amphibolites GQAB 14, GQAB 25, AB 41 and AB 77-A: these samples are slightly enriched in LREE with respect to MREE ($[La/Sm]_n$ = 1,07-1,43) and a little more relative to HREE ($[La/Yb]_n$ = 1,46-2,42). Two subgroup patterns can be highlighted, based in Eu contents and LREE/HFSE ratios:

(1A) The samples AB 41 and AB 77-A present negative anomalies in Eu ([Eu/Eu*] = 0,76-0,85), possibly due to fractionation of plagioclase. The LREE is slightly enriched relative to Nb ($[La/Nb]_n$ = 1,62-1,75) and highly enriched in LREE relatively to Th ($[La/Th]_n$ = 5,31-5,46).

(1B) The samples GQAB 14 and GQAB 25 do not present negative anomalies in Eu ([Eu/Eu*] = 0,97-1,07). The LREE is slightly enriched relative to Nb ($[La/Nb]_n$ = 1,80-2,11) and Th ($[La/Th]_n$ = 1,01-1,62).

In general, all the samples are depleted in more incompatible HFSE as Th, Nb and Ta (GQAB 14 presents Th, La and Ce contents slightly higher) relatively to less incompatible HFSE (Y, Tm, Yb), presenting REE patterns similar with those mentioned for anorogenic basalts such as N-MORB to T-MORB (Sun *et al.*, 1979; Sun and McDonough, 1989).

(2) Amphibolites GQAB 19, AB 40, AB 46 and AB 48: these samples do not present negative anomalies in Eu (Eu/Eu*] = 0,96-1,05). They are enriched in LREE with respect to MREE ($[La/Sm]_n$ = 1,90-2,24) and highly enriched in LREE and MREE relatively to HREE ($[La/Yb]_n$ = 7,50-9,00; $[Sm/Yb]_n$ = 3,35-422). As respect to the LREE and other HFSE relation, the LREE are slightly depleted relative to Nb ($[La/Nb]_n$ = 0,81-0,97) and slightly enriched relative to Th ($[La/Th]_n$ =

1,45-1,57). These samples present a similar pattern of incompatible elements being enriched in more incompatible HFSE (Th, Nb, Ta, La, Ce) relatively to the less incompatible (Ti, Tb, Y, Tm, Yb), which are similar to the E-MORB and OIB patterns (e.g. Sun *et al.*, 1979; Sun and McDonough, 1989).

The discrimination between these two groups is also clear in Zr/Y and Ti/Y ratios (Fig. 12A): group (1) has Zr/Y = 3,44-5,27 and Ti/Y = 293,28-413,82, while group (2) has Zr/Y = 7,65-10,81 and Ti/Y = 575,96-911,30. The Pearce and Gale (1977) and Pearce (1982; 1983) diagrams (Fig. 12A), based on previous mentioned ratios, assign the group (1) to plate margin basalts, while the group (2) are associated with within-plate magmatism.

The group (1) samples also show the previous subdivision based on Eu anomaly and LREE/HFSE ratios: the subgroup (1A), with Zr/Y = 4,84-5,27, is projected in within-plate basalts field, near the MORB field, while subgroup (1B), with Zr/Y = 3,44-3,60, is projected within MORB field (Fig. 12A). The group (2) shows higher values of Zr/Y (7,65-10,81), being projected in within-plate basalts field (Fig. 12A). Despite these variations, the data plot of the analysed mafic rocks in the Ti-Zr diagram (Pearce, 1982; Fig. 12A) show a tholeiitic trend ([Ti/Zr] = 81±9), between MORB and within plate component.

The ratios Th/Yb vs Ta/Yb discriminant diagram (Fig. 12B; Pearce, 1982) also show the two mentioned groups: the group (1) presents lower values of Ta/Yb (0,08-0,12) and Th/Yb (0,05-0,34) being projected in MORB field (subgroup (1A): [Ta/Yb] = 0,08-0,12; [Th/Yb] =0,05-0,08) and in volcanic arc-basalts near from MORB and within plate tholeiites fields (subgroup (1B): [Ta/Yb] = 0,09-0,10; [Th/Yb] = 0,16-0,34), while the group (2) samples presents higher values of Ta/Yb (0,82-1,08) and Th/Yb (0,86-0,99), being plotted in the within-plate magmatism field (Fig. 12B).

The Hf-Th-Ta (Wood, 1980) ternary discriminant diagrams allows to a better characterization of tectonic setting (Fig. 12C). The amphibolites from group (1) have a Hf/Ta = 7,50-13,60. The subgroup (1A) with highest values of Hf/Ta (10,00-13,60) is projected in the N-MORB field, while the subgroup (1B), with Hf/Ta=7,50-9,38, is plotted within N-MORB field, near the boundary with volcanic-arc basalts, and in the volcanic-arc basalts field. The samples from group (2) have a Hf/Ta ratio ranging between 2,46 and 3,25, being projected in E-MORB to within-plate tholeiites fields (Fig. 12C).

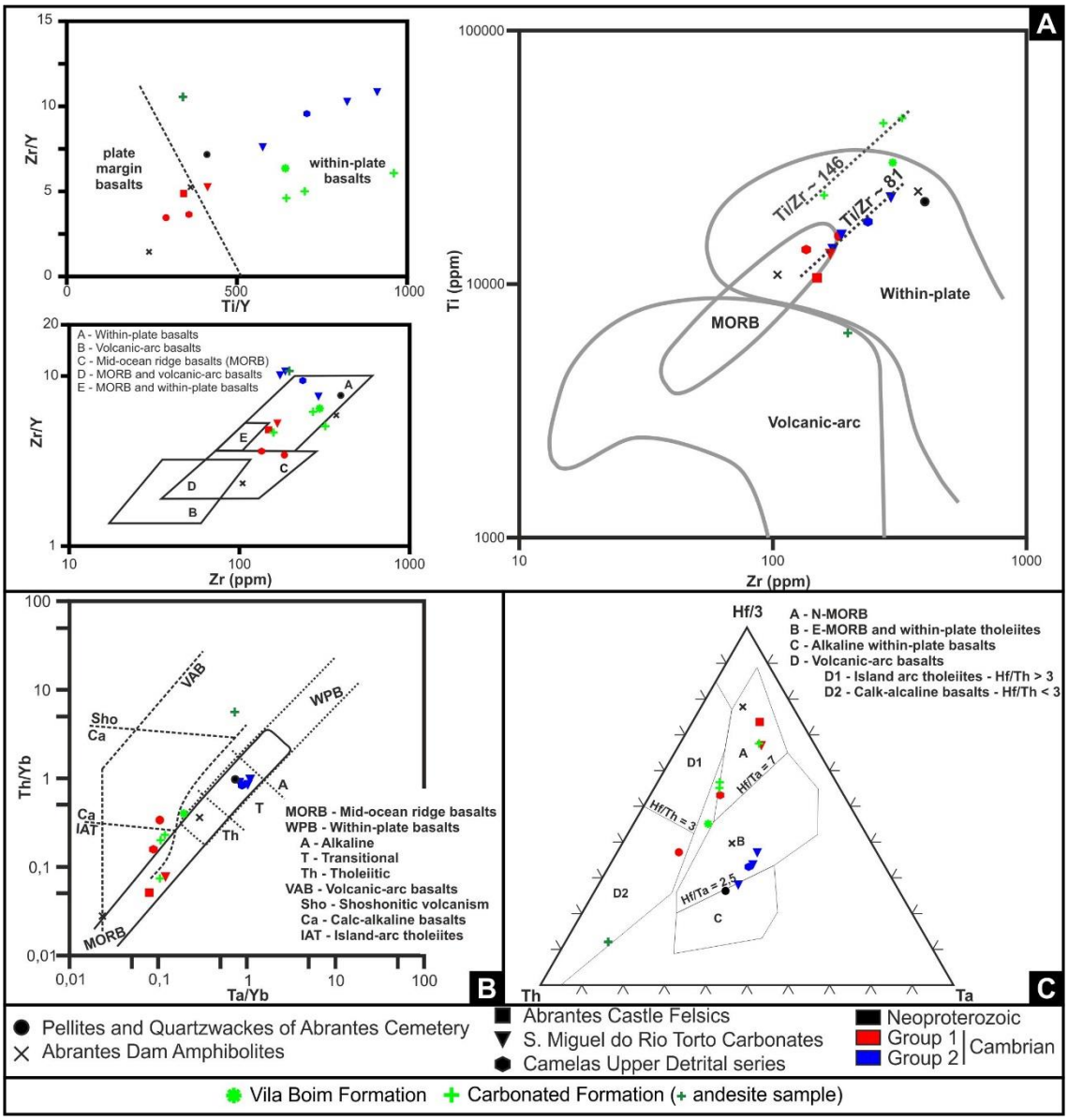

Figure 12 – Discriminant diagrams used to mafic derived volcanic rocks:

A – Ti, Zr and Y relation diagrams (adapted from Pearce and Gale, 1977; Pearce, 1982; 1983);

B – Th/Yb vs Ta/Yb diagram (adapted from Pearce, 1982);

C – Hf-Th-Ta ternary diagram (adapted from Wood, 1980).

II.2.4.3.2. Vila Boim volcanic rocks

The Vila Boim samples show higher dispersion in its geochemical nature. The Alkalis contents vs SiO_2 (Le Maitre *et al.*, 1989; Fig. 9A1) recognize two felsic (rhyolites - VB 10, VB 11), one intermediate (andesite - VB 01) and four mafic rocks (two basalts – VB 06, VB 07 –, one tephrite-basanite – VB 05 – and one trachy-basalt – VB 16). The rhyolites display high contents in SiO_2 (75,40-77,30%) and lower TiO_2 (0,45-0,67%), $Fe_2O_{3(tot)}$ (0,71-0,77%), MgO (0,05-0,68%) and Al_2O_3 (13,32-14,40%) when compared with intermediate (SIO_2 57,84%; TiO_2 0,64%; $Fe_2O_{3(tot)}$ 6,83%;

MgO 5,12%; Al_2O_3 16,99%) and mafic ones (SIO_2 44,77-48,53%; TiO_2 2,25-4,52%; $Fe_2O_{3(tot)}$ 12,27-15,32%; MgO 4,57-6,63%; Al_2O_3 14,67-15,66%). The rhyolites presents high content in Na_2O (7,36-7,54%) and lower K_2O (0,02-0,03%) and CaO (0,36-0,60%), when compared with intermediate (Na_2O 2,39%; K_2O 2,72%; CaO 7,24%) and mafic (Na_2O 2,94-5,18%; K_2O 0,09-0,71%; CaO 7,29-13,43%) volcanics,

The obtained data shows that felsic rocks are subalkaline with homogeneous Alkalis contents (7,38-7,57%; Fig. 9A1), being projected in calc-alkaline series in AFM diagram (Fig. 9A2). Mafic rocks are plotted on alkaline and subalkaline fields with Alkalis ranging from 3,06-5,56% and the intermediate rock is projected in alkaline field, showing 5,11% of Alkalis content (Fig. 9A1). The mafic and intermediate rocks are projected near the Irvine and Baragar (1971) curve in the AFM diagram (Fig. 9A2), being clearly enriched in MgO, specially the samples VB 01 and VB 06. The samples VB 01, VB 05 and VB 16 are projected in calk-alcaline field while the samples VB 06 and VB 07 are projected in tholeiitic field.

The rhyolites are peraluminous, presenting ASI between 3,06 and 3,16. Nevertheless, the sample VB10 is a ferroan-rhyolite and the VB11 is a magnessian-rhyolite, being clearly enriched in MgO when compared with VB10 (table II).

Although the mafic rocks presents distinct geochemical nature, there are no substantial variations on major elements contents. The tephrite-basanite is quite similar to basalts, with higher content in $Fe_2O_{3(tot)}$ (12,27-15,32%), CaO (8,30-13,43%), MgO (4,57-6,63%), TiO_2 (2,25-4,52), being poor in K_2O (0,09-0,12). The trachy-basalt from Vila Boim Formation (VB 16) is only distinguish from the other mafic samples because have higher K_2O values (0,71%) and lower CaO content (7,29%), being the other major elements clear similar.

The #Mg for the mafic samples range between 29,59-32,84 (VB05, VB07 and VB16) and 40,45 (VB 06), which reflect the higher content in MgO (6,63%) relatively to Fe2O3(tot) (12,80%) in VB 06 basalt. The enrichment in MgO is accompanied by a depletion in Na_2O and TiO_2 contents in this sample, which is the main distinctive feature of VB 06 basalt.

The REE patterns of Vila Boim rhyolites, plotted in a normalized primitive mantle diagram (Fig. 10C), display negative anomalies in Eu (Eu/Eu* = 0,38-0,66). They are enriched in LREE with respect to MREE and HREE ($[La/Sm]_n$ = 1,38 to 4,35; $[La/Yb]_n$ = 2,06 to 13,58).

The sample VB 11 is enriched in LREE relatively to Nb ($[La/Nb]_n$ =3,24) and depleted relative to Th ($[La/Th]_n$ = 0,32), while in the VB 10, LREE is depleted relative to Nb and highly depleted relative to Th ($[La/Nb]_n$ = 0,63, $[La/Th]_n$ =0,04). The HFSE normalized primitive mantle diagram (Fig. 10D) display similar patterns for the rhyolite samples with enrichments in the more incompatible HFSE (i.e. Th, Ta) relatively to the less incompatible HFSE (i.e. Tb, Y, Tm, Yb). It must

to be emphasized the presence of Nb and Sm negative anomaly in both samples and an enrichment in Zr and Hf. Some distinctive features are identified in rhyolite samples: the sample VB 10 is generally more enriched in HFSE elements, with exception to La and Ce, showing positive anomaly in Ta and negative anomaly in La and Ti, which are not identified in sample VB 11.

The rhyolites show a Th/Ta ratio range between 14,8 and 17,0, similar to those observed in the rhyolites from the active continental margins (Fig. 11A; Gordon and Schandl, 2000). Similar features are assigned by Nb-Y and Ta-Yb discriminant diagram (Fig. 11B; Pearce *et al.*, 1984).

The mafic and intermediate volcanic rocks data are plotted in a primitive mantle normalized REE and HSFE diagrams (Fig. 10G and 10H) display two distinct patterns:

(1) Andesite (VB 01): it is enriched in LREE with respect to MREE and to HREE ($[La/Sm]_n$ = 3,96; $[La/Yb]_n$ = 13,94). The sample present negative anomaly in Eu ([Eu/Eu*] = 0,76), possibly due to fractionation of plagioclase, being enriched in LREE relative to Nb ($[La/Nb]_n$ = 1,99) and depleted relative to Th ($[La/Th]_n$ = 0,42). The sample is enriched in Th, Ta and La relatively to less incompatible HFSE (Tb, Y, Tm, Yb). The HFSE pattern shows negative anomalies in Nd, Sm and Ti.

(2) Mafic rocks (VB 05, VB 06, VB 07 and VB 16): although the REE patterns are quite similar, two distinct behaviours are identified as respect to Eu anomaly: the sample VB-06 do not present Eu anomaly Eu ([Eu/Eu*] = 1,06) while the other samples presents a slightly negative anomaly (Eu (Eu/Eu*] =0,84-0,92). The VB 06 sample do not shows clear enrichement of LREE relative to MREE ($[La/Sm]_n$ = 1,18), being enriched relative to HREE ($[La/Yb]_n$ = 2,01), while the samples with Eu negative anomaly are slightly enriched in LREE with respect to MREE and to HREE ($[La/Sm]_n$ = 1,53-1,63; $[La/Yb]_n$ = 2,70-2,90), being slightly enriched in MREE relatively to HREE ($[Sm/Yb]_n$ = 1,70-1,78). This slightly differentiation is also clear in LREE-HFSE relation: the sample VB 06 are slightly enriched in LREE relatively to Nb ($[La/Nb]_n$ = 1,69) and highly enriched in Th ($[La/Th]_n$ =4,91) while the other samples are equally enriched in LREE relatively to Nb and Th ($[La/Nb]_n$ = 1,39-2,70; $[La/Th]_n$ = 1,17-2,50). The diagram are uniform for all the mafic rocks, presenting a horizontal pattern, being slightly enrichment in more incompatible HFSE (i.e. Th, Nb, Ta) relatively to the less incompatible HFSE (i.e. Y, Tm, Yb). The sample VB 06 presents clear depletion in Th relatively to less incompatible HFSE (Tb, Y, Tm, Yb). The patterns also show slightly positive anomalies in La and Zr, slightly negative anomalies in Sm and Hf, and clear positive anomaly in Ti. The general patterns are similar with the N-MORB to T-MORB patterns (e.g. Sun *et al.*, 1979; Sun and McDonough, 1989).

The projection of mafic rocks in the discriminant diagrams of Pearce and Gale, (1977) and Pearce (1982; 1983) indicates a within plate origin for these mafic rocks (Fig. 12A). As in Abrantes samples, also here a linear trend is defined in the Ti-Zr diagram ([Ti/Zr] = 146±3; Pearce, 1982), although in this case the ratio is higher, resulting from Ti enrichement in this samples. The Th/Yb vs Ta/Yb discriminant diagram (Fig. 12B; Pearce, 1982) show a slightly distinct geochemical fingerprint: the sample VB-06 is projected in MORB field (Ta/Yb = 0,11 and Th/Yb= 0,07), while the other samples are projected in volcanica-arc basalts field, near the boundary of MORB (VB 05 and VB 07) and within plate basalts (VB 16) fields (Ta/Yb = 0,11-0,19 and Th/Yb= 0,20-0,40). Similar behaviour is also identified in Hf-Th-Ta ternary discriminant diagram (Wood, 1980): sample VB 06 is projected in N-MORB field, the samples VB 05 and VB 07 are projected in N-MORB field, near the boundary with volcanic-arc basalts, and the sample VB 16 projected near the boundary between N-MORB, E-MORB - within-plate tholeiites and volcanic-arc fields (Fig. 12C). All the samples presents a Hf/Ta higher than 7 (7,46-11,40) typical of N-MORB's. The andesite sample present a discrepant behaviour, being generally projected in volcanic-arc fields (Fig. 12).

II.2.4.3.3. Discussion of geochemical data

The mafic and one of the felsic rocks sampled in Neoproterozoic assigned units from Abrantes presents anorogenic features. Exception to GQAB 16 metadacite, which present higher values of Th/Ta ratio, presenting an orogenic fingerprint (Gordon and Schandle, 2000).

According to Gordon and Schandl (2000), the increase of Th in felsic rocks is attributed to the contribution of a volcanic-arc component related with convergent margins (i.e. volcanic rocks are more enriched in Th with respect to Ta in subduction zones than in within-plate and mid-oceanic ridge volcanism). The enrichment in Th/Ta ratios in GQAB 16 could be interpreted by two distinct ways:

- the two dacite samples are related with the same anorogenic process and the differences can be explained due by heterogeneities in magmatic sources. According to this possibility, the GQAB 16 metadacite melting source could be a subtract with orogenic features, being enriched in Th relative to Ta, or
- the samples represents two distinct geodynamical processes acting during the Neoproterozoic times, firstly anorogenic followed by an orogenic process.

Although the amphibolites present uniform geochemical features, with anorogenic tholeiitic features, the sample GQAB 5A presents N-MORB features and the other two samples a tholeiitic (to transitional) within-plate basalts. This fact seems to show the presence of crustal stretching

processes during Neoproterozoic times, possibly related to Cadomian Cycle. Similar features are also described in other ortho-derived amphibilites as in Montemolín (Eguíluz *et al.*, 1990; Gómez-Pugnaire *et al.*, 2003; Sanchez Lorda *et al.*, 2014) and Besteiros (Ribeiro *et al.*, 2003), also attributed to Neoproterozoic.

The mafic and felsic samples sampled in Cambrian attributed units from Abrantes and from Vila Boim show geochemical features which seems to display that they are linked to continental rifting processes.

The rhyolites present higher values of Th/Ta, typical of active continental margins (Gordon and Schandle, 2000), which is also compatible with the relations between Nb-Y and Yb-Ta proposed by Pearce *et al.* (1984). However, the geological setting of these samples is not compatible with this geological ambience.

The application of discrimination diagram to first steps of Cambrian felsic volcanism is complex, since the melts generated by continental crust melting depends on the thickness and sources of continental crust composition and also the incompatibility of Th, Nb, Ta, Y and Yb, as reported by Pearce *et al.* (1984). Indeed, these kind of behaviour were also reported by Mata and Munhá, (1990) and Sánchez-Garcia *et al.*, (2008; 2010) for cambrian metarhyollites in other sectors of OMZ (Fig. 11B), being also interpreted as relate to the first steps of Variscan Cambrian extension.

The spatial (and temporal) association between felsic and mafic volcanic rocks shows a possible relation to the same geodynamic process. Indeed, all the mafic rocks, sampled in Cambrian attributed units from Abrantes and Vila Boim, present anorogenic fingerprints. The mafic rocks samples from Abrantes and Vila Boim show typical tholeiitic trend, with association between within-plate and MORB-like basalts. This trend is evident in Th/Yb-Ta/Yb, Zr/Y-Ti/Y and Ti-Zr diagram of Pearce (1982; 1983) and Pearce and Gale (1977), which seems to show that they are co-genetic.

The geochemical data shows two distinct groups in mafic rocks based in REE content:

- N-MORB to T-MORB, sometimes with negative anomalies in Eu and a slightly enrichment in Th. This fact could result from the magma migration process, followed by a differentiation process with crystallization of plagioclase. During the migration process, the magma could have contamination with continental crust rocks, which could explain the enrichment in Th. This possibility could explain the projection of some samples within or near from volcanic-arc basalts field on Wood (1980) and Pearce (1982) diagrams (Fig. 12), and

- a group more enriched in LREE relative to previously mentioned, that contain a REE and HFSE patterns similar to E-MORB/OIB. The discriminant diagrams corroborate its tholeiitic anorogenic fingerprint, attributing a within-plate nature to these mafic rocks.

In summary, the samples collected in Cambrian attributed units from both localities presents tholeiitic anorogenic features, presenting bimodal nature, emphasizing the continental stretching during Cambrian times, compatible with Variscan Ocean opening during Ordovician Times (Pedro *et al.*, 2010; Sánchez-Garcia *et al.*, 2010).

II.2.5. Stratigraphic Correlation Analysis

The stratigraphic succession described for the Abrantes region shows similarities with the Neoproterozoic-Cambrian sequences defined for diverse sectors of the OMZ, such as the Alter-do-Chão-Elvas domain, where Vila Boim samples are provided. Due to the absence of geochronological and paleontological data supporting the stratigraphic correlations, the proposal assigning ages for the units forming the Abrantes stratigraphic succession will be based on standard lithostratigraphic relationships with Neoproterozoic-Lower Cambrian stratigraphic sequences established for other sectors of this paleogeographic zone (*e.g.* Liñan and Quesada, 1990; Oliveira *et al.*, 1991; Gozalo *et al.*, 2003; Etxebarria *et al.*, 2006; Pereira *et al.*, 2006; Araújo *et al.*, 2013; Fig. 13 and 14), also using the geochemical data from volcanic rocks to strengthen this correlation.

The Abrantes Neoproterozoic assigned units could be correlate with units included in the Neoproterozoic *Série Negra* Group of the NE Alentejo sector (*e.g.* Quesada *et al.*, 1990; Oliveira *et al.*, 1991; Eguíluz *et al.*, 1995) and the Olivenza-Monesterio Antiform (*e.g.* Eguíluz *et al.*, 1990; 1995; 2000; Schäfer *et al.*, 1993; Quesada *et al.*, 1990;. Ordoñez-Casado *et al.*, 2009). Indeed, the general features displayed by the Abrantes Cemetery Pelites and Quartzwackes are similar to those typifying the basal units of *Série Negra*, such as the Morenos and Montemolín Formations (Fig. 9 and 10).

The Abrantes Dam Amphibolites, with a geochemistry from the N-MORB's to the within plate tholeiitic basalts, should trace an important episode of mafic volcanism in Abrantes region during Neoproterozoic times. Similar lithostratigraphic and geochemical features are also described in the Neoproterozoic sections forming the OMZ northern sectors, either in Portugal (Besteiros Amphibolites; *e.g.* Ribeiro *et al.*, 2003; Pereira *et al.*, 2006) or in Spain (Las Mesas, El Cuartel and Montemolin Amphibolites; Abalos and Eguíluz, 1989; Eguíluz *et al.*, 1990; 1995; 2000; Ordoñez-Casado, 1998; Sanchez Lorda *et al.*, 2014; 2016). Although in some places in

Northern OMZ, basalts with volcanic-arc geochemistry are also identified associated to N-MORB's to the within plate tholeiitic basalts (Sanchez Lorda *et al.*, 2014).

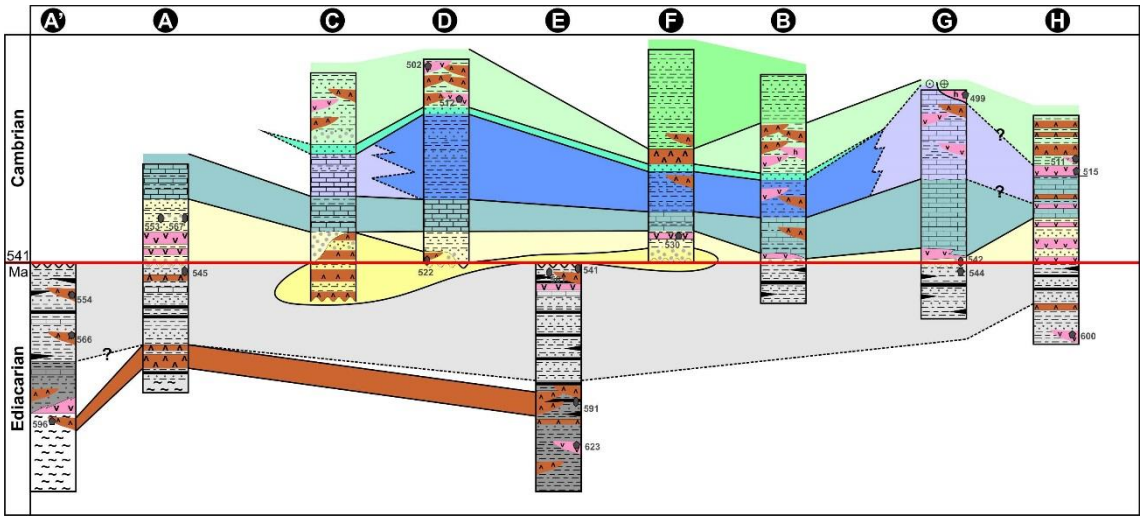

Figure 13 – Stratigraphic correlation diagram of the Neoproterozoic and Cambrian lithostratigraphic units in the OMZ (see Fig. 2 for the legend and location of stratigraphic charts).

As in Abrantes, the Montemolin amphibolites are interspersed in metapelite series (Sanchez Lorda *et al.*, 2014). In Olivença-Monestério Anticline, a maximum deposition time span around 590-580 Ma is proposed, thus constraining the age of the amphibolite sequence (Schafer *et al.*, 1989; 1990; Ordoñez-Casado, 1998). In addition to the previously mentioned data it should be noted that the Abrantes Dam Amphibolites is intruded by a gneissic granite (Maiorga Granite; Fig. 14) dated of 482±79 Ma (Rb-Sr, whole rock; Serrano Pinto, 1984) and, more recently, of 569±6 Ma (SHRIMP U-Pb in zircon; Mateus *et al.*, 2015), attesting its possible age.

Over the amphibolite-dominant unit and in apparent stratigraphic continuity, the Abrantes *Série Negra s.s.* are deposited, being characterized by the presence of flints (sometimes named as black metacherts or black quartzites in other sections), within dark-coloured metapelites and metagreywackes series, occasionally with subordinate amphibolites.

This lithological diversity is described in classical works (Alia, 1963; Carvalhosa, 1965; Vegas, 1968) as one of the main lithological features in the *Série Negra* succession. Thus, the Abrantes *Série Negra s.s.* could be correlated with the Mosteiros and Tentudia Formations (*e.g.* Eguíluz *et al.*, 1990; 1995; 2000; Quesada *et al.*, 1990; Oliveira *et al.*, 1991; Schäfer *et al.*, 1993).

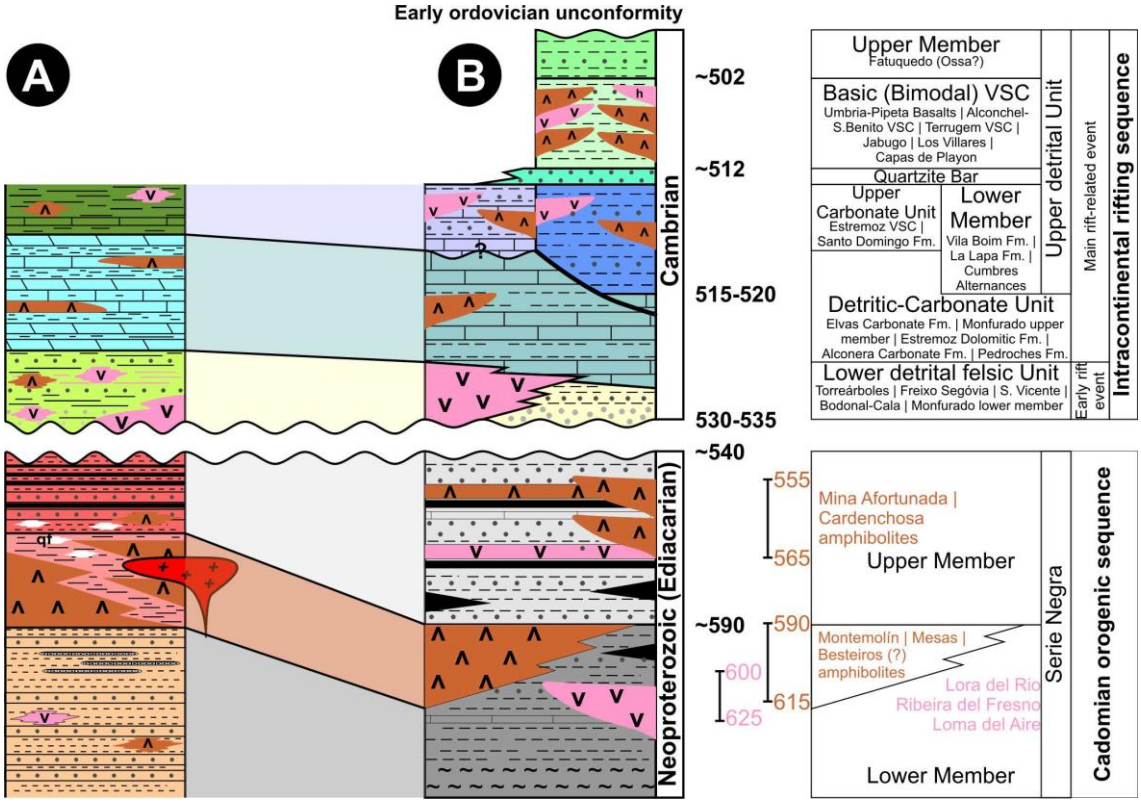

Figure 14 – Proposed general lithostratigraphic column for the Neoproterozoic-Cambrian of OMZ (adapted from Pereira *et al.*, 2011 and Nance *et al.*, 2012) and the correlation with lithostratigraphic column preserved in the Abrantes region.

As respect to the Cambrian related units, geochemical, petrologic, petrographic and stratigraphic features displayed by the Abrantes Castle Felsics support its correlation with S. Vicente, Freixo-Segovia and Nave de Grou-Azeiteiros volcano-sedimentary complexes (Pereira and Silva, 2006; Pereira *et al.*, 2006; 2011; Sanchez-Garcia *et al.*, 2010), as well with the lower member of the Monfurado Formation (Montemor-Ficalho sector; Chichorro *et al.*, 2008; Fig. 13) and the Torreárboles Formation and the Bodonal-Cala volcano-sedimentary complex (Quesada *et al.*, 1990; Eguíluz *et al.*, 2000; Gozalo *et al.*, 2003; Sanchez-Garcia *et al.*, 2003; 2008; 2010). Geochronological studies indicates a Lower Cambrian for these units, scattered in the 530-520 Ma time window (Pereira *et al.*, 2006;. 2012a; Romeo *et al.*, 2006; Chichorro *et al.*, 2008; Linnemann *et al.*, 2008; Alvaro *et al.*, 2014; Fig. 13 and 14).

The OMZ Early Cambrian felsic volcanism presents volcanic-arc signature (Mata and Munhá, 1990; Sanchez-Garcia *et al.*, 2008) that is also reported in studied felsic samples, resulting from its orogenic melting sources. The coarse-grained lithotypes, typical of Cambrian basal units, are poorly preserved in study area, excepting in its eastern sectors (near the Barca Pego; Fig. 1B) where levels of meta-arkoses and meta-conglomerates can be observed without ambiguity (Fig.

13). The discontinuous character of the basal conglomerate is reported in other OMZ sectors and, in these cases, the Carbonated Units are deposited directly over the Neoproterozoic succession (*e.g.* Liñan and Quesada, 1990; Oliveira *et al.*, 1991; Gozalo *et al.*, 2003; Creveling *et al.*, 2013).

Geological mapping (Fig. 3) shows that Abrantes Castel Felsics contact with all Neoproterozoic assigned units, which seems to be symptomatic of a deformation episode affecting only the Neoproterozoic assigned units in Abrantes region (possibly resulting from Cadomian orogeny), which is also emphasized by early deformation episodes noted in Abrantes Cemetery Pelites and Quartzwackes Unit. However, this assumption needs to be seen with caution, since the contacts between Cambrian and the Neoproterozoic units are structural demarked by Variscan shear zones.

The S. Miguel do Rio Torto Carbonates, developed over the previous volcano-sedimentary sequence in apparent stratigraphic continuity, correlates suitably with the Elvas Carbonated and Estremoz Dolomite Formations and the Assumar and Ouguela Detrital-Carbonate Complexes (Oliveira *et al.*, 1991; Pereira *et al.*, 2006; 2012a; Moreira *et al.*, 2014b; 2016), as well as with the Detrital-Carbonated Unit present in Alconchel, Alconera and Pedroches (*e.g.* Gozalo *et al.*, 2003; Sanchez-Garcia *et al.*, 2010; Creveling *et al.*, 2013; Fig. 13 and 14). These units are composed of crystalline dolomite and calcite marbles and limestones, which are interbedded with mafic volcanic rocks. The analysed mafic rocks in the S. Miguel do Rio Torto Carbonates unit display geochemical features compatible with within plate to MORB geochemistry, which is in accordance with the geochemical fingerprints identified in similar units, such as in Alter-do-Chão-Elvas, in Zafra-Alconera or in Alconchel-Jerez successions (Mata and Munhá, 1990; Sanchez-Garcia *et al.*, 2008; 2010). These carbonate-rich units are assigned to the Lower Cambrian (Ovetian-Lower Marianian, Series 2), based on its fossiliferous content (*e.g.* Liñan and Quesada, 1990; Gozalo *et al.*, 2003; Creveling *et al.*, 2013). Recent isotopic studies also indicate similar $^{87}Sr/^{86}Sr$ ratios for the Abrantes and other Cambrian carbonates from OMZ (Moreira *et al.*, 2016).

Overlaying the S. Miguel do Rio Torto Carbonates, also in stratigraphic continuity, a poorly represented upper siliciclastic unit with interleaved bimodal meta-volcanic rocks (mafic prevailing over felsic terms) can be observed and the mafic rocks also present tholeiitic fingerprint. This upper unit presents some similarities with the top detrital(-carbonate) sequence reported in Pedroches succession (NE Spain; Santo Domingo Formation; *e.g.* Liñan and Quesada, 1990; Gozalo *et al.*, 2003; Creveling *et al.*, 2013; Fig. 13 and 14). However, it is not reported the presence of significant volcanic rocks in Santo Domingo Formation, which also

present a higher abundance of carbonate layers. Accepting this correlation, the age of the Camelas Upper Detrital Series should be ascribed to Marianian. Note that equivalent time span is represented in basal sections of siliciclastic successions overlapping the carbonate-rich units cropping out in the Alter-do-Chão-Elvas-Cumbres Mayores Domain (Vila Boim, La Lapa Formations and Cumbres Alternances; Delgado, 1905; Liñan and Quesada, 1990; Oliveira *et al.*, 1991; Gozalo *et al.*, 2003; Creveling *et al.*, 2013). In these siliciclastic Formations, also with Marianian age, the bimodal volcanic rocks are recognized (Oliveira *et al.*, 1991; Gozalo *et al.*, 2003), showing that volcanic processes are active during sedimentation of Camelas Upper Detrital Series, which could explain the presence of bimodal volcanic rocks in this unit.

II.2.6. Geodynamic evolution

This section propose a model for the Neoproterozoic and Cambrian evolution of OMZ, which try to integrate the new Abrantes data with previous models of the Iberian Variscides.

The generation of a Neoproterozoic volcanic-arc in the northern margin of Gondwana induced by the subduction of Iapetus below the southern continent is consensual (Fig. 15A; Eguilluz *et al*., 2000; Ballèvre *et al*., 2001; Ribeiro *et al*., 2007; Linnemann *et al*., 2008). However, its location is debatable. While some consider it was developed south (in current coordinates) of the OMZ, resulting from Iapetus subduction (Ballèvre *et al*., 2001; Murphy *et al*., 2004; Linnemann *et al*., 2008; Sanchez-Lorda *et al*., 2014), the presence of Neoproterozoic HT and HP metamorphic rocks along the TBCSZ led others to considered this first other structure as the Cadomian suture (Ribeiro *et al*., 2009). The Neoproterozoic sequence, included in Série Negra Group, with a lower member formed by siliciclastic rocks with some calco-silicate and limestone layers, suggests a deposition in a relatively energetic shallow marine environment. The younger zircons find in this member suggests a maximum deposition around 590-580 Ma (Ordoñez-Casado *et al*., 2009).

The volcanic-arc magmatism is sometimes considered to be represented in Northern OMZ, by the calc-alkaline basalts with Early Ediacarian age (ca. 630-590 Ma; Sanchez-Lorda *et al*., 2014). These conclusion seems incongruent with a passive margin environment of the Série Negra lower member, indicated by its anorogenic bimodal volcanism typical from a within-plate magmatic settings. An alternative proposal consider the deposition of this member in the back-arc basin developed over the the thinned Gondwana margin, which may contain evidences of calc-alkaline magmatism related to volcanic-arc magmatism (Fig. 16A). This environment could also explain the anorogenic bimodal volcanic rocks enclosed in this member, that could result from the beginning of continental stretching related with this back-arc basin (Fig. 16B).

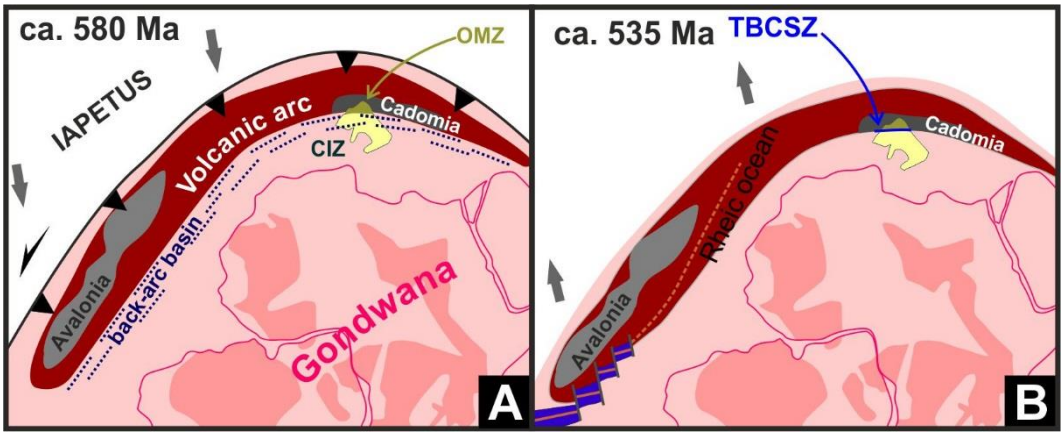

Figure 15 – Proposal of paleogeographic reconstitution of North-Gondwana margin during (A) Neoproterozoic and (B) Lower Cambrian times (adapted from Murphy *et al*., 2004; Pereira *et al.*, 2006; Linnemann *et al*., 2008).

This is compatible with the association between the volcanic arc calc-alkaline basalts with N-MOR and E-MOR basalts with a 580 Ma age (Lorda-Sanchez *et al*., 2014). Such age is in accordance, not only with the time span for the back-arc-basin formation (ca. 590-550 Ma; Linnemann *et al*., 2008), but also with the presence of dioritic and granitic plutonism with similar ages (ca. 580-570Ma; Ordoñez-Casado, 1998; Bandrés *et al*., 2004).

The progression of the back-arc stretching led to the overlap of the previous shallow and energetic marine sequence by a significant tholeiitic volcanism. Such volcanism induced the formation of abundant mafic rocks, now represented by the amphibolites of Abrantes Dam, Besteiros, Las Mesas and Montemolín (Eguíluz *et al*., 1990; Quesada *et al*., 1990; Ribeiro *et al*., 2003; Sanchez-Lorda *et al*., 2014). These amphibolites could represent the evolution of the anorogenic magmatism related with the back-arc lithospheric stretching (Fig. 16B), which is supported by their E-MORB to N-MORB signature. This process could have generated oceanization in the back-arc basin (Fig. 16C). This small ocean were developed in the northern domain of OMZ, separating two distinct basements in Iberia: the OMZ one, with a strong Cadomian imprint, and the CIZ one, where Cadomian magmatism and deformation is negligible.

The oceanization in back-arc basins, with generation of MORB-like basalts is observed in relation to the Mariana Trough induced by the Pacific subduction (Gribble *et al*., 1998; Pearce and Stern, 2006; Oakley *et al*., 2009).

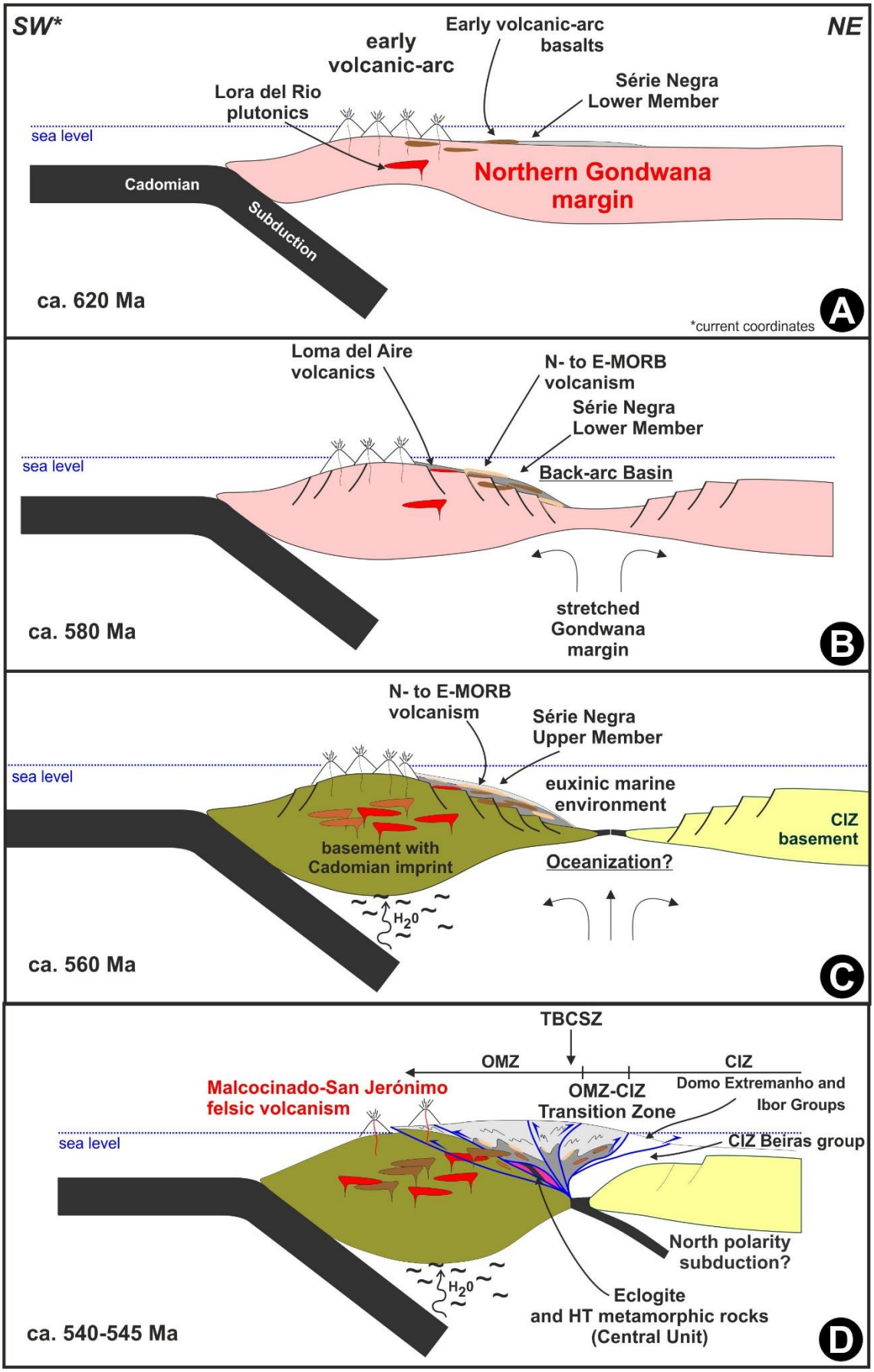
SW*
NE
early volcanic-arc
Early volcanic-arc basalts
Série Negra Lower Member
Lora del Rio plutonics
sea level
Cadomian
Subduction
Northern Gondwana margin
ca. 620 Ma
*current coordinates
A
Loma del Aire volcanics
N- to E-MORB volcanism
Série Negra Lower Member
sea level
Back-arc Basin
stretched Gondwana margin
ca. 580 Ma
B
N- to E-MORB volcanism
Série Negra Upper Member
sea level
euxinic marine environment
CIZ basement
basement with Cadomian imprint
Oceanization?
H2O
ca. 560 Ma
C
TBCSZ
OMZ
CIZ
Malcocinado-San Jerónimo felsic volcanism
OMZ-CIZ Transition Zone
Domo Extremanho and Ibor Groups
sea level
CIZ Beiras group
North polarity subduction?
H2O
Eclogite and HT metamorphic rocks (Central Unit)
ca. 540-545 Ma
D

Figure 16 – Main stages in the Ediacarian evolution of OMZ (includes data from Abalos *et al*., 1991; Linnemann *et al*., 2008; Ribeiro *et al*., 2007; Sanchez-Lorda *et al*., 2014; Jensen and Palacios, 2016):

A – Generation of an early volcanic-arc, associated to plutonism;

B – Beginning of the back-arc basin opening, with generation of MORB-like volcanic rocks;

C – Oceanization of the back-arc basin, related with Cadomian subduction;

D – Upper Ediacarian inversion of the back-arc, with the development of a cryptic structure along the TBCSZ, and the last pulses of Cadomian magmatism.

Above this OMZ magmatic event, begins the deposition of the Upper Member of Série Negra Group, a flyschoid sequence of greywackes interlayered with black shales and black quartzites (flints). These features indicate a deeper marine euxinic environment (continental slope or transition continental shelf-slope; Walker, 1976; Stow and Shanmugam, 1980) compatible with the deposition of Série Negra Upper Member in a confined back-arc basin (Fig. 16C).

During Upper Ediacarian times (ca. 545-540 Ma), the inversion of the back-arc basin deformed previous succession giving rise to the Cadomian Orogeny (Fig. 15B and 16D). The Malcocinado and San Jerónimo Formations, could represent the last pulses of the Cadomian chain volcanism, which was accompanied between 550 and 530 Ma by plutonism (Fig. 16D; Salman, 2004; Simancas *et al*., 2004). This inversion also deformed the Ediacarian Units from the southern CIZ domains that have been deposit in the back-arc basin (Domo Extremanho and Ibor Groups; Palacios *et al*., 2013; Eguiluz *et al*., 2015; 2016; Jensen and Palacios, 2016; Fig. 16D).

Although the presence of a back-arc basin between OMZ and CIZ, with possible small oceanization, during the Ediacarian seems inescapable, it should have been very narrow, as shown by the isotopic similarities between the Ediacarian detrital successions of both zones, proving that they have never been substantially separated during that time (Lopez-Guijarro *et al*., 2008).

The inversion of the back-arc basin also explains, not only the presence of Late Ediacarian granulites but also Cadomian HP rocks associated to the TBCSZ. This lithospheric structure are reactivated during the Variscan Cycle as an intraplate shear zone, controlling the Early Variscan structure of OMZ (Fig. 16D; Abalos, 1992; Abalos *et al*., 1992; Ribeiro *et al*., 2009; Romão *et al*., 2010; Henriques *et al*., 2015).

During the Lower Cambrian (ca. 525 Ma), began the crustal stretching related with the early stages of the Variscan Cycle and the coeval deposition of the OMZ Cambrian sequence, which includes the Abrantes Group succession. During the early intracontinental rifting, occurs

the deposition of a detrital volcano-sedimentary complex with arkoses and conglomerates, which corresponds to the molasses of the Cadomian Orogenic Chain (Fig. 17A). Associated to these clastic deposits an intense calc-alkaline felsic magmatism are produced (Mata and Munhá, 1990; Ordoñez-Casado *et al*., 1998; Pereira *et al*., 2006; López-Guijarro *et al*., 2008; Sanchez-Garcia *et al*., 2010), due to the melting of the Cadomian lithosphere. This geochemical signature emphasize the orogenic nature of the Cadomian melted crust and not the temporal extension of orogenic processes.

The transition from the late stages of the Cadomian Cycle to the early steps of the Variscan intracontinental rifting seems to be almost continuous (Simancas *et al*., 2004). This could indicate that the beginning of the Variscan Cycle might be related with the Cadomian high heat flow, due to the asthenospheric upwelling associated with the Cadomian slab break-off (?). Such process could explain, both the emplacement of mantle derived magmatic rocks during lower Cambrian (Culebrín tonalite, 532 ± 4 Ma Pb-Pb in zircon; Salman, 2004) and the Late Cadomian ages of the HT metamorphism (ca. 540-510 Ma; Eguíluz *et al*., 2000 and references therein; Henriques *et al*., 2015).

After the deposition of the Lower Cambrian (Ovetian-Marianian) volcano-siliciclastic complexes, a wide marine carbonate platform were established, from the region of Abrantes-Assumar-Pedroches region, towards the southern domains of OMZ (Montemor-Ficalho-Aracena; Fig. 17B). Locally, in the carbonate shelf a mafic volcanism with within-plate to MORB geochemistry is found. This shows that the crustal thinning related with the continental rifting continues during the carbonated sedimentation. Moreover, the presence of limestones emphasizes the continuity of marine environment in the syn-rift basins. The abundance of impure dolomite-rich limestones bellow the shallow carbonated shelf is recognize in several syn-rift succession (e.g. Kullberg *et al*., 2013; Martín-Martín e al., 2013; Ershova *et al*., 2016).

After the deposition of the carbonate dolomite-rich sediments, the progression of the intracontinental rifting develops two distinct depositional environments in the OMZ (Fig. 17C):

- In Alter-do-Chão-Elvas-Cumbres Mayores domain predominate the deep facies represented by flysch-type lithotypes, associated to bimodal volcanism (ca. 515-510 Ma);
- In the northern (Abrantes-Pedroches) and southern domains (Estremoz-Ficalho-Escoural) the shallow marine sedimentation were dominant. In Estremoz and Ficalho a second carbonated unit were formed, while in Escoural and Abrantes-Pedroches a gradual transition between carbonated and siliciclastic sedimentation is found. In both domains the sedimentation is coeval of a bimodal volcanism.

Previous zoning seems to indicate the presence of two distinct marine sedimentary environments during this stage (Fig. 17C): in the deepest, the clastic flyschoid sedimentation prevails, while in the shallow one the carbonated and thin-grained sedimentation is pervasive.

The MORB-like mafic dykes in the Neoproterozoic and Lower Cambrian units are related to the Lower Palaeozoic intracontinental rifting (Oliveira *et al*., 1991; Sanchez-Garcia *et al*., 2003; 2008; 2010; Etxebarria *et al*., 2006; Lopez-Guijarro *et al*., 2008). These volcanic rocks dykes, intruding the Neoproterozoic units, represent the Cambrian volcanism feeding channels.

The intracontinental rifting process culminates in the Upper-Cambrian-Lower Ordovician with the opening of a Variscan Ocean in the southwest of the OMZ margin (Pedro *et al*., 2010; Sanchez-Garcia *et al*., 2010; Moreira *et al*., 2014a). This tectonic environment is compatible with the Upper Cambrian sedimentary unconformity pervasive in the OMZ (Oliveira *et al*., 1991; Gozalo *et al*., 2003).

It should be emphasized that the recognition of a typical OMZ Neoproterozoic-Cambrian transition sequence in the Abrantes region is of major importance, because it allows to place the OMZ-CIZ boundary to the NE of Olalhas-Sardoal-Mouriscas sector, as already proposed by Romão *et al*. (2014).

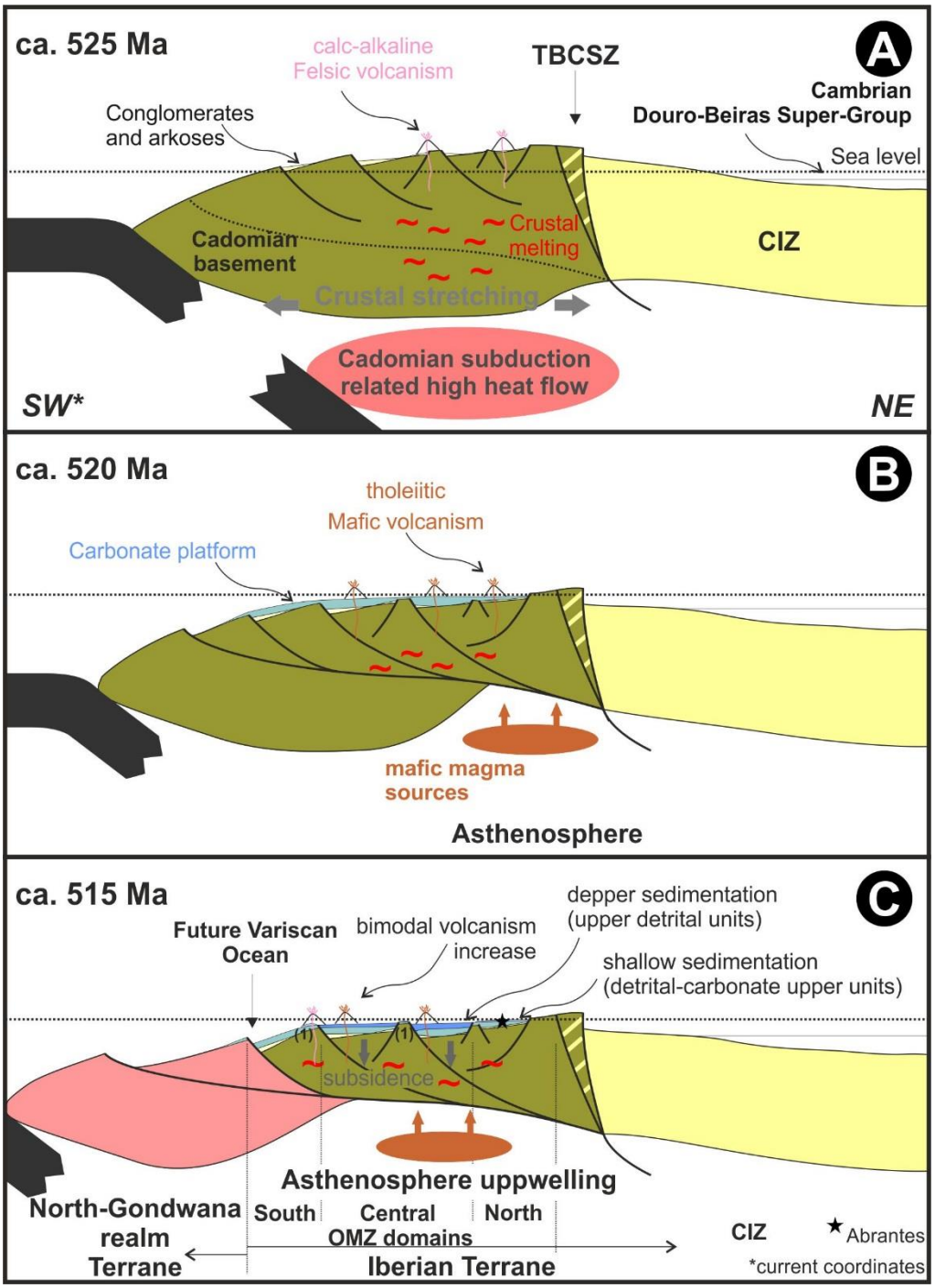

Figure 17 – Proposed Lower to Middle Cambrian evolution of OMZ, emphasising the beginning of North Gondwana lithosphere stretching related to the onset of the Variscan Cycle (includes data from Linnemann *et al*., 2008; Ribeiro *et al*., 2007; Moreira *et al*., 2014b; Jensen and Palacios, 2016):

A – The early felsic magmatic pulse, with calc-alkaline signature resulting from melting of the Cadomian crust;

B – Tholeiitic magmas are related to asthenospheric sources contemporaneous shallow carbonated sedimentation;

C – The lateral and vertical variations of the stratigraphic sequence due the depth of basin related with its subsidence during crustal stretching.

References

Abalos, B. (1992). Variscan shear-zone deFormation of a late Precambrian basement in SW Ibéria: implications for Circum-Atlantic Pre-Mesozoic tectonics. Journal of Structural Geology 14(7), 807-823. DOI: 10.1016/0191-8141(92)90042-U

Abalos, B., Eguíluz, L. (1989). Structural analysis and deformed early lineations in Black quartzites from the central Badajoz-Cordoba shear zone (Iberian Variscan Fold Belt), Rev. Soc. Gel. España, 2 (1-2), 95-102.

Abalos, B., Eguíluz, L., Apalategui, O. (1990). Constituición ectono-estratigráfica del Corredor Blastomilonítico de Badajoz-Córdoba: nueva proposta de subdivicion. Geogaceta, 7, 71-72.

Abalos, B., Gil Ibarguchi, J.I., Eguíluz, L. (1991). Cadomian subduction/collision and Variscan transpression in the Badajoz-Córdoba shear belt, southwest Spain. Tectonophysics 199, 51-72. DOI: 10.1016/0040-1951(91)90118-C

Alía, M. (1963): Rasgos estructurales de la Baja Extremadura. Bol Real Soc Esp Hist Nat 61:247–262

Álvaro, J.J., Bellido, F., Gasquet, D., Pereira, M.F., Quesada, C., Sánchez-García, T., (2014). Diachronism in the late Neoproterozoic–Cambrian arc-rift transition of North Gondwana: A comparison of Morocco and the Iberian Ossa-Morena Zone. Journal of African Earth Sciences, 98, 113-132. DOI: 10.1016/j.jafrearsci.2014.03.024

Apalategui, O., Eguíluz, L., Quesada, C. (1990). Ossa-Morena zone: structure. In: Dallmeyer, R.D., Martínez-García, E. (Eds.), Pre-Mesozoic Geology of Iberia. Springer-Verlag, Berlin-Heidelberg, Germany, pp. 280–292.

Araújo, A., Piçarra de Almeida, J., Borrego, J., Pedro, J., Oliveira, J.T. (2013). As regiões central e sul da Zona de Ossa-Morena, in: Dias, R., Araújo, A., Terrinha, P., Kullberg, J.C. (Eds.), Geologia de Portugal (Vol. I), Escolar Editora, Lisboa, 509-549.

Ballèvre, M., Le Goff, E., Hébert, R. (2001). The tectonothermal evolution of the Cadomian beld of Northern Britanny, France: Neoproterozoic volcanic arc. Tectonophisics, 331, 19-43. DOI: 10.1016/S0040-1951(00)00234-1

Bandrés, A., Eguíluz, L., Pin, C., Paquette, J.L., Ordónez-Casado, B., Le Fèvre, B., Ortega, L.A., Gil Ibarguchi, J.I. (2004). The northern Ossa-Morena Cadomian batholith (Iberian Massif): magmatic arc origin and early evolution. International Journal of Earth Sciences 93, 860–885. DOI: 10.1007/s00531-004-0423-6

Bellon, H., blachere, H., Crousilles, M., Deloche, C., Dixsaut, C., Hertricht, B., Prostdame, V., Rossi, Ph., Simon, D., Tamain, G. (1979). Radiochronologie, évolution tectono-magmatique et implications métallogénetiques dans les Cadomo-Variscides du Sud-Est hespérique. Bulletin Societé Géologique France, 21, 113-120.

Carvalho, D., Goínhas, J., Oliveira, V., Ribeiro, A. (1971). Observações sobre a geologia do Sul de Portugal e consequências metalogenéticas. Est. Not. Trabalhos, Serv. Fom. Mineiro, 20, 1-2, 153-199.

Carvalhosa, A. (1965). Contribuição para o conhecimento geológico da região entre Portel e Ficalho (Alentejo). Memorias dos Serviços Geológicos de Portugal 11, 1-130.

Carvalhosa, A., Gonçalves, F., Oliveira, V. (1987). Notícia explicativa da folha 36-D, Redondo. Serviços Geológicos de Portugal.

Chichorro, M., Pereira, M.F., Díaz-Azpiroz, M., Williams, I.S., Fernandez, C., Pin, C., Silva, J.B. (2008). Cambrian ensialic rift-related magmatism in the Ossa-Morena Zone (Évora-Aracena metamorphic belt, SW Iberian Massif): Sm-Nd isotopes and SHRIMP zircão U-Th-Pb geochronology. Tectonophysics 461, 91-113. DOI:10.1016/j.tecto.2008.01.008

Coelho, A., Gonçalves, F. (1970). Rocha hiperalcalina de Estremoz. Bol. Soc. Geol. Portugal, XVII, 181-185.

Conde, L. (1984). Excursão geológica na região de Ferreira do Zêzere-Abrantes. VI Reunião do Grupo de Ossa Morena, Livro-guia, 1-8, Universidade de Coimbra.

Creveling, J.R., Fernández-Remolar, D., Rodríguez-Martínez, M., Menéndez, S., Bergmann, K.D., Gill, B.C., Abelson, J. Amils, R., Ehlmann, B.L., García-Bellido, D.C, Grotzinger, J.P., Hallmann, C., Stack, K.M., Knoll, A.H. (2013). Geobiology of a Lower Cambrian Carbonate Platform, Pedroche Formation, Ossa Morena Zone, Spain. Palaeogeography, Palaeoclimatology, Palaeoecology 386, 459-478. DOI:10.1016/j.palaeo.2013.06.015

Delgado, J.F.N. (1905). Contribuições para o estudo dos terrenos paleozóicos. I. Precâmbrico e Arcaico; II. Câmbrico. Com. Serv. Geol. Portugal 7, 56-122.

Eguíluz L., Gil Ibarguchi J.I., Abalos B., Apraiz A. (2000). Superposed Hercynian and Cadomian orogenic cycles in the OssaMorena zone and related areas of the Iberian Massif. Geol. Soc. Am. Bull., 112: 1398-1413.

Eguíluz, L., Abalos, B., Ortega, L.A. (1990). Anfibolitas proterozoicas del sector central de la zona de Ossa Morena. Geoquímica e implicaciones geodinâmicas. Cuaderno Lab. Xeolóxico de Laxe. 15, 119-131

Eguíluz. L., Apraiz, A., Abalos, A., Martinez-Torres, L.M. (1995). Evolution de la zone d'Ossa Morena (Espegne) au cous du proterozoique superior: corrélations acec l'orogène cadomien nord armoricain. Geológie de la France, 3, 35-47.

Eguiluz L. Martinez-Torres L.M., Sarrionadia F., Carracedo M., Gil-Ibarguchi J.I. (2015). The Ibero-Armorican Belt: an evolving island-arc along northern Gondwana between ca. 650 and 480 Ma. Geólogie de la France, 2015(1), 58-59.

Eguiluz, L., Palacios, T., Jensen S., Sarrionandia, F. (2016). La Zona Centro Iberica Meridional: Cuenca tras-arco del orogeno cadomiense del Norte de Gondwana. Geoguias, 10, 55-88

Ershova, V.B., Prokopiev, A.V., Khud, A.K. (2016). Devonian–Permian sedimentary basins and paleogeography of the Eastern Russian Arctic: An overview. Tectonophysics 691(A), 234-255. DOI: 10.1016/j.tecto.2016.03.026

Etxebarria M., Chalot-Prat F., Apraiz A., Eguíluz L. (2006). Birth of a volcanic passive margin in Cambrian time: Rift paleogeography of the Ossa-Morena Zone, SW Spain. Precamb. Res., 147: 366-386. DOI:10.1016/j.precamres.2006.01.022

Fernández-Suárez, J., Gutiérrez-Alonso, G., Jeffries, T.E. (2002). The importance of along margin terrane transport in northern Gondwana: insights from detrital zircon parentage in Neoproterozoic rocks from Iberia and Brittany. Earth and Planetary Science Letters 204, 75–88. DOI:10.1016/S0012-821X(02)00963-9

Frost, B.R., Barnes, C.G., Collins, W.J., Arculus, R.J., Ellis, D.J., Frost, C.D. (2001). A Geochemical Classification for Granitic Rocks. J. Petrol., 42 (11), 2033-2048. DOI: 10.1093/petrology/42.11.2033

Gómez-Pugnaire, M., Azor, A., Fernández-Soler, J., Sánchez Vizcaíno, V. L. (2003). The amphibolites from the Ossa-Morena/Central Iberian Variscan suture (Southwestern Iberian Massif): Geochemistry and tectonic interpretation, Lithos, 68, 23 – 42. DOI:10.1016/S0024-4937(03)00018-5

Gonçalves, F., Zbyszewski, G., Carvalhosa, A., Coelho, A. (1979). Carta Geológica de Portugal 1:50 000, folha 27-D (Abrantes). Serv. Geol. Portugal, Lisboa.

Gorton M.P., Schandl E.S. (2000). From continents to island arcs: a geochemical index of tectonic setting for arc-related and within-plate felsic to intermediate volcanic rocks. The Canadian Mineralogist, 38, 1065-1073. DOI: 10.2113/gscanmin.38.5.1065

Gozalo, R., Liñán, E., Palacios, T., Gámezvintaned, J.A., Mayoral, E. (2003). The Cambrian of the Iberian Peninsula: an overview. Geologica Acta 1, 103–112.

Gribble R.F., Stern, R.J. Newman, S., Bloomer, S.H, O'hearn, T. (1998). Chemical and Isotopic Composition of Lavas from the Northern Mariana Trough: Implications for Magmagenesis in Back-arc Basins. Journal of Petrology 39(1), 125–154. DOI: 10.1093/petroj/39.1.125

Henriques, S.B.A., Neiva, A.M.R., Ribeiro, M.L., Dunning, G.R., Tajčmanová, L., (2015). Evolution of a Neoproterozoic suture in the Iberian Massif, Central Portugal: New U-Pb ages of igneous and metamorphic events at the contact between the Ossa Morena Zone and Central Iberian Zone. Lithos 220-233, 43-59. DOI:10.1016/j.lithos.2015.02.001

Irvine, T.N., Baragar, W.R.A. (1971). A guide to the chemical classification of the common volcanic rocks: Canadian Journal of Earth Sciences, 8, 523-548. DOI: 10.1139/e71-055

Jensen, S., Palacios, T. (2016). The Ediacaran-Cambrian trace fossil record in the Central Iberian Zone, Iberian Peninsula. Comunicações Geológicas, 103(I), 83-92.

Julivert, M., Fontboté, J.M., Ribeiro, A., Conde, L.E. (1974). Memória Explicativa del Mapa Tectónico de la Península Ibérica y Baleares. Instituto Geológico y Minero de España, Madrid, 113 pp.

Kullberg, J. C., Rocha, R. B., Soares, A. F., Rey, J., Terrinha, P., Azerêdo, A. C., Callapez, P., Duarte, L. V., Kullberg, M. C., Martins, L., Miranda, J. R., Alves, C., Mata, J., Madeira, J., Mateus, O., Moreira, M., Nogueira, C. R. (2013). A Bacia Lusitaniana: Estratigrafia, Paleogeografia e Tectónica. In: R. Dias, A. Araújo, P. Terrinha, J.C. Kullberg (Eds), Geologia de Portugal, vol. 2, Escolar Editora, 195-347.

Le Maitre, R. W. (Editor), Bateman, P,, Dudek, A., Keller, J. Er Al. (1989). A Classification of Igneous rocks and Glossary of Term: Recommendations of the International Union of Geological Sciences Subcommission on the Systematics of Igneous Rocks. Blackwell Scientific Publications, Oxford

Liñán, E., Álvaro, J., Gozalo, R., Gámez-Vintaned, J.A., Palacios, T. (1995). El Cámbrico Medio de la Sierra de Córdoba (Ossa-Morena, S de España): trilobites y paleoicnología. Implicaciones bioestratigráficas y paleoambientales. Revista Española de Paleontología, 10 (2), 219-238.

Liñán, E., Quesada, C. (1990). Ossa-Morena Zone: Stratigraphy, in: Dallmeyer, R.D., Martinez Garcia, E. (Eds.) Pre-Mesozoic Geology of Iberia. Springer-Verlag, Berlin, 229–266.

Linnemann, U., Pereira, M.F., Jeffries, T., Drost, K., Gerdes, A. (2008). Cadomian Orogeny and the opening of the Rheic Ocean: New insights in the diacrony of geotectonic processes constrained by LA-ICP-MS U-Pb zircão dating (Ossa-Morena and Saxo-Thuringian Zones, Iberian and Bohemian Massifs)". Tectonophysics 361, 21-43. DOI:10.1016/j.tecto.2008.05.002

Lopes, J.L. (2003). Contribuição para o conhecimento Tectono-Estratigráfico do Nordeste Alentejano, transversal Terena-Elvas. Implicações económicas no aproveitamento de rochas ornamentais existentes na região (Mármores e Granitos). PhD Thesis (unpublished), Évora University, Portugal 568 pp.

López-Guijarro, R., Armendáriz M., Quesada C., Fernández-Suárez J., Murphy, J. B, Pin,C., Bellido, F. (2008). Ediacaran–Palaeozoic tectonic evolution of the Ossa Morena and Central Iberian zones (SW Iberia) as revealed by Sm–Nd isotope systematics. Tectonophysics 461, 202–214. DOI:10.1016/j.tecto.2008.06.006

Lötze, F. (1945): Zur Gliederung der Varisciden der Iberishen Meseta. Geoteckt Forsch, vol. 6, pp.78-92.

Martín-Martín, J.D., Gomez-Rivas, E., Bover-Arnal, T., Travéa, A., Salas, R., Moreno-Bedmar, J.A., Tomás, S., Corbella, M., Teixell, A., Vergés, J., Stafford, S.L. (2013). The Upper Aptian to Lower Albian syn-rift carbonate succession of the southern Maestrat Basin (Spain): Facies architecture and fault-controlled stratabound dolostones. Cretaceous research 41, 217-236. DOI: 10.1016/j.cretres.2012.12.008

Mata, J., Munhá, J. (1985). Geochemistry of mafic volcanic rocks from the Estremoz region (South Central Portugal). Comunicações dos Serviços geológicos de Portugal, 71(2), 175-185.

Mata, J., Munhá, J., (1990). Magmatogénese de metavulcanitos câmbricos do nordeste alentejano: os estádios iniciais de "rifting" continental. Comun. Serv. Geol. Portugal 76, 61-89.

Mateus, A., Mata, J., Tassinari, C., Rodrigues, P., Ribeiro, A., Romão, J., Moreira, N., (2015). Conciliating U-Pb SHRIMP Zircon Dating with Zircon Saturation and Ti-in-Zircon Thermometry in the Maiorga and Endreiros Granites (Ossa-Morena Zone, Portugal). X Congresso Ibérico de Geoquímica, Laboratório Nacional de Energia e Geologia, Lisboa, 38-41.

Mette, W. (1989). Acritarchs from Lower Paleozoic rocks of the Western Sierra Morena (SW Spain) and biostratigraphic results. Geologica et Paleontologica, Merburg, 53: 1-19.

Moreira, N. (2012). Caracterização estrutural da zona de cisalhamento Tomar-Badajoz-Córdova no sector de Abrantes. Unpublished MsC thesis, University of Évora, 225 p.

Moreira, N., Araújo, A., Pedro, J.C., Dias, R. (2014a). Evolução geodinâmica da Zona de Ossa-Morena no contexto do SW Ibérico durante o Ciclo Varisco. Comunicações geológicas 101 (Vol. Especial I), 275-278.

Moreira, N., Dias, R., Pedro, J.C., Araújo, A. (2014b). Interferência de fases de deformação Varisca na estrutura de Torre de Cabedal; sector de Alter-do-Chão – Elvas na Zona de Ossa-Morena. Comunicações geológicas 101 (Vol. Especial I), 279-282.

Moreira, N., Pedro, J., Romão, J., Dias, R., Araújo, A. Ribeiro A. (2015). The Neoproterozoic-Cambrian transition in Abrantes Region (Central Portugal); Litostratigraphic correlation with Cambrian Series of Ossa-Morena Zone. The Variscan belt: correlations and plate dinamics. Géologie de la France (Variscan 2015 special issue, Rennes), 2015(1), 101-102. ISBN:978-2-7159-2612-7.

Moreira, N., Pedro, J., Santos, J.F., Araújo, A., Romão, J., Dias, R., Ribeiro, A., Ribeiro, S., Mirão, J. (2016). $^{87}Sr/^{86}Sr$ ratios discrimination applied to the main Paleozoic carbonate sedimentation in Ossa-Morena Zone. In: IX Congreso Geológico de España (special volume). Geo-Temas, 16(1), 161-164. ISSN 1576-5172.

Murphy , J. B., Pisarevsky, S. A., Nance, R. D., Keppie, J. D. (2004). Neoproterozoic–Early Palaeozoic evolution of peri-Gondwanan terranes: implications for Laurentia–Gondwana connections. International Journal of Earth Sciences 93, 659–82. DOI: 10.1007/s00531-004-0412-9

Nance, R.D., Gutiérrez-Alonso, G., Keppie, J.D., Linnemann, U., Murphy, J.B., Quesada, C., Strachan, R.A., Woodcock, N.H. (2012). A brief history of the Rheic Ocean. Geoscience Frontiers 3, 125-135. DOI:10.1016/j.gsf.2011.11.008

Oakley, A. J., Taylor, B., Moore, G. F., Goodliffe, A. (2009). Sedimentary, volcanic, and tectonic processes of the central Mariana Arc: Mariana Trough back-arc basin Formation and the West Mariana Ridge. Geochemistry Geophysics Geosystems, 10(8), Q08X07, DOI:10.1029/2008GC002312

Oliveira, D. P. S., Reed, R. M., Milliken, K. L., Robb, L. J., Inverno, C. M. C., D'Orey, F. L. C. (2003). *Série Negra* black quartzites – Tomar Cordoba Shear Zone, E Portugal: mineralogy and cathodoluminescence studies. Cadernos Lab. Xeolóxico de Laxe, 28, 193-211.

Oliveira, J.T., Oliveira, V., Piçarra, J.M. (1991). Traços gerais da evolução tectono-estratigráfica da Zona de Ossa Morena, em Portugal: síntese crítica do estado actual dos conhecimentos. Comun. Serv. Geol. Port. 77, 3-26.

Oliveira, V.M. (1984). Contribuição para o conhecimento geológico-mineiro da regiao de Alandroal-Juromenha (Alto Alentejo). Est. Not. Trab., Serv. Fom. Mineiro XXVI (1-4): 103-126.

Ordóñez Casado, B. (1998). Geochronological studies of the Pre-Mesozoic basement of the Iberian Massif: the Ossa-Morena Zone and the Allochthonous Complexes within the Central Iberian Zone. PhD Thesis ETH Zurich, 235 p.

Ordoñez-Casado, B., Gebauer, D., Eguíluz, L. (1998). SHRIMP age-constraints for the calc-alkaline volcanism in the Olivenza-Monesterio Antiform (Ossa Morena, SW Spain). Goldschmidt Conference, Toulouse. Mineralogical Magazine, 62A, 1112-1113.

Ordoñez-Casado, B., Gebauer, D., Eguíluz, L. (2009). Zircão Ion-Probe Dating the Maximum Age of Deposition of the Montemolín Succession (Lower *Série Negra*) in the Ossa Morena Zone, Spain. Macla, 11, 137-138

Palacios, T. Eguiluz, L., Apalategui, A. (2013). Geological Map of Estremadura (1:350.000) and descriptive memory. UPV-EHU, Bilbao, 222p.

Pearce, J.A. (1982). Trace element characteristics of lavas from destructive plate boundaries. In: Thorpe, R. S. (ed.), Andesites. New York: John Wiley & Sons, 525-548.

Pearce, J.A. (1983). Role of the sub-continental lithosphere in magma genesis at active continental margins. In: Hawkesworth, C.J. and Norry, M.J. eds.Continental basalts and mantle xenoliths, Nantwich, Cheshire: Shiva Publications, pp. 230-249.

Pearce, J.A., Gale, G. H. (1977). Identification of ore-deposition environment from trace element geochemistry of associated igneous host rocks. In: Volcanic Processes in Ore Genesis. Spec. Publ. Inst. Min. Metall. And Geol. Soc. London, 14-24. 10.1144/GSL.SP.1977.007.01.03

Pearce, J.A., Stern R.J. (2006). Origin of Back-Arc Basin Magmas: Trace Element and Isotope Perspectives. Geophysical Monograph Series 166, 63-86. DOI: 10.1029/166GM06

Pearce, J.A., Harris, N.B.W., Tindle, A.G. (1984). Trace element discrimination diagrams for the tectonic interpretation of granitic rocks. J. Petrol., 25 (4), 956-983. DOI: 10.1093/petrology/25.4.956

Pedro, J. C., Araújo, A., Tassinari, C., Fonseca, P. E., Ribeiro, A. (2010). Geochemistry and U-Pb zircão age of the Internal Ossa-Morena Zone Ophiolite Sequences: a remnant of Rheic Ocean in SW Iberia, Ofioliti 35 (2), 117-130. WOS:000285862100004.

Perdigão, J. (1967). Estudos geológicos na Pedreira de Mestre André (Barrancos). Comun. Serv. Geol. Portugal 52.

Pereira, M.F., Silva, J.B. (2006). Nordeste Alentejano, In R. Dias, A. Araújo, P. Terrinha, J. Kullberg (Eds.) Geologia de Portugal no Contexto da Ibéria. Uni. Evora, Evora, p. 145-150

Pereira, M.F., Chichorro, M., Linnemann, U., Eguíluz, L., Silva, J.B. (2006). Inherited arc signature in Ediacaran and Early Cambrian basins of the Ossa-Morena Zone (Iberian Massif, Portugal): paleogeographic link with European and North African Cadomian correlatives. Precambrian Research, 144, 297-315. DOI:10.1016/j.precamres.2005.11.011

Pereira, M.F., Apraiz, A., Chichorro, M., Silva, J.B., Armstrong, R.A. (2010a). Exhumation of high-pressure rocks in northern Gondwana during the Early Carboniferours (Coimbra-Cordoba shear zone, SW Iberian Massif): tectonothermal analysis and U-Th-Pb SHRIMP in-situ zircon geochronology. Gondwana Research, 17(2), 440-460. DOI:10.1016/j.gr.2009.10.001

Pereira, M.F., Silva, J.B., Drost, K., Chichorro, M., Apraiz, A. (2010b). Relative timing of transcurrent displacements in northern Gondwana: U–Pb laser ablation ICP-MS zircão and monazite geochronology of gneisses and sheared granites from the western Iberian Massif (Portugal). Gondwana Research, 17, 461–481. DOI:10.1016/j.gr.2009.08.006

Pereira, M.F., Chichorro, M., Sola, A.R., Silva, J.B., Sanchez-Garcia, T., Bellido, F., (2011). Tracing the Cadomian magmatism with detrital/inherited zircão ages by in-situ U-Pb SHRIMP geochronology (Ossa-Morena Zone, SW Iberian Massif).Lithos 123(1-4), 204-217. DOI: 10.1016/j.lithos.2010.11.008

Pereira, M.F., Solá, A.R., Chichorro, M., Lopes, L., Gerdes, A., Silva, J.B., (2012a). North-Gondwana assembly, break up and paleogeography: U–Pb isotope evidence from detrital and igneous zircãos of Ediacaran and Cambrian rocks of SW Iberia. Gondwana Research 22(3–4), 866-881. DOI:10.1016/j.gr.2012.02.010

Pereira, M.F., Silva, J.B., Chichorro, M., Ordóñez-Casado, B., Lee, J.K.W., Williams, I.S., (2012b). Early Carboniferous wrenching, exhumation of high-grade metamorphic rocks and basin instability in SW Iberia: constraints

derived from structural geology and U-Pb and 40Ar-39Ar geochronology. Tectonophysics 558-559, 28-44 DOI:10.1016/j.tecto.2012.06.020

Piçarra, J.M. (2000). Estudo estratigráfico do sector de Estremoz-Barrancos, Zona de Ossa Morena, Portugal. Vol. I - .Litoestratigrafia do intervalo Câmbrico médio?-Devónico inferior, Vol. II - Bioestratigrafia do intervalo Ordovícico-Devónico inferior. PhD Thesis (unpublished), Évora University, Portugal.

Piçarra, J.M., Le Meen, J. (1994). Ocorrência de crinóides em mármores do Complexo Vulcano-Sedimentar Carbonatado de Estremoz: implicações estratigráficas. Comunicações do Instituto Geológico e Mineiro 80, 15-25

Pin, Ch., Liñán, E., Pascual, E., Donaire, T., Valenzuela, A. (2002). Late Neoproterozoic crustal growth in the European variscides: Nd isotope and geochemical evidence from the Sierra de Córdoba andesites (Ossa-Morena Zone, Southern Spain). Tectonophysics 352, 133-151. DOI:10.1016/S0040-1951(02)00193-2

Quesada, C. (1991). Geological constraints on the Palaeozoic tectonic evolution of tectonostratigraphic terranes in the Iberian Massif. Tectonophysics 185, 225-245. DOI: 10.1016/0040-1951(91)90446-Y

Quesada, C., Apalategui, O., Eguíluz, L., Liñan, E., Palácios, T. (1990). Ossa-Morena Zone. Precambrian. In R. D. Dallmeyer, E. Martinez (Eds.). Pre-Mesozoic Geology of Iberia. Springer Verla, Berlin, pp. 252- 258.

Ribeiro, A., Antunes, M. T., Ferreira, M. P., Rocha, R. B., Soares, A. F., Zbyszewski, G., Moitinho de Almeida, F., Carvalho, D., Monteiro, J. H. (1979). Introduction à la géologie générale du Portugal. Serviços Geológicos de Portugal, 114 p.

Ribeiro, A., Munhá, J., Dias, R., Mateus, A., Pereira, E., Ribeiro, L., Fonseca, P., Araújo, A., Oliveira, T., Romão, J., Chaminé, H., Coke, C., Pedro, J. (2007). Geodynamic evolution of SW Europe Variscides. Tectonics 26, TC6009. DOI: 10.1029/2006TC002058

Ribeiro, A., Pereira, E., Fonseca, P., Mateus, A., Araújo, A., Munhá, J., Romão, J. Rodrigues, J. F., Castro, P., Meireles, C., Ferreira, N. (2009). Mechanics of thick-skinned Variscan overprinting of Cadomian basement (Iberian Variscides). C. R. Geosciences, Paris 341 (2-3), 127-139. DOI: 10.1016/j.crte.2008.12.003

Ribeiro, A., Quesada, C., Dallmeyer, R. D. (1990). Geodynamic evolution of the Iberian Massif. In R. D. Dallmeyer, E. Martínez García (Eds.) Pre- Mesozoic Geology of Iberia. Springer-Verlag, pp. 397-410.

Ribeiro, M.L., Pereira, M.F., Solá, A.R. (2003). O ciclo Cadomiano na ZOM: Evidências geoquímicas. Congresso Ibérico de Geoquimica. Universidade de Coimbra, Portugal, 102–104.

Rollinson, H. (1993). Using Geochemical Data: evaluation, presentation, interpretation, p. 102-212

Romão, J., Ribeiro, A., Munhá, J., Ribeiro, L. (2010). Basement nappes on the NE boundary the Ossa-Morena Zone (SW Iberian Variscides). European Geosciences Union, General Assembly, Vienna, Austria (Abstract).

Romão, J., Moreira, N., Dias, R., Pedro, J., Mateus, A., Ribeiro, A. (2014). Tectonoestratigrafia do Terreno Ibérico no sector Tomar-Sardoal-Ferreira do Zêzere e relações com o Terreno Finisterra. Comunicações Geológicas 101 (Vol. Especial I), 559-562

Romeo, I., Lunar, R., Capote, R., Quesada, C., Dunning, G.R., Piña, R., Ortega, L., (2006). U/Pb age constraints on Variscan Magmatism and Ni-Cu-PGE metallogeny in the Ossa-Morena Zone (SW Iberia). Journal of the Geological Society of London 163, 837-846. DOI: 10.1144/0016-76492005-065

Salman, K. (2004). The timing of the Cadomian and Variscan cycles in the Ossa-Morena Zone, SW Iberia: granitic magmatism from subduction to extension. Journal of Iberian Geology 30, 119-132.

Sánchez Carretero, R., Eguíluz, L., Pascual, E., Carracedo, M. (1990). Ossa-Morena Zone: Igneous rocks. In: Dallmeyer, R. D. and Martínez García, E., (eds.), Pre-Mesozoic Geology of Iberia, Springer Verlag, Berlin: 292-313.

Sánchez-García, T., Bellido, F., Pereira, M.F., Chichorro, M., Quesada, C., Pin, C., Silva, J.B. (2010). Rift-related volcanism predating the birth of the Rheic Ocean (Ossa-Morena zone, SW Iberia). Gondwana Research 17, 392–407. DOI:10.1016/j.gr.2009.10.005

Sánchez-García, T., Bellindo, F., Quesada, C. (2003). Geodynamic setting and geochemical signatures of Cambrian-Ordovician rift-related igneous rocks (Ossa-Morena Zone, SW Iberia). Tectonophysics 365, pp. 233-255. DOI:10.1016/S0040-1951(03)00024-6

Sánchez-García, T., Quesada, C., Bellido, F., Dunning, G.R., González de Tánago, J. (2008). Two-step magma flooding of the upper crust during rifting: the Early Palaeozoic of the Ossa Morena Zone (SW Iberia). Tectonophysics 461, 72–90.

Sánchez-García, T., Quesada, C., Dunning, G.R., Perejón, A., Bellido, F., Moreno-Eiris, E. (2007). New geochronological and geochemical data of the Loma del Aire Unit, Ossa- Morena Zone. IGCP 497-Galicia Meeting 2007. Publicaciones del IGME, 164–165. DOI:10.1016/j.tecto.2008.03.006

Sanchez-Lorda, M.E., Sarrionandia, F., Ábalos, B., Carrracedo, M., Eguíluz, L., Gil Ibarguchi, J.I. (2014). Geochemistry and paleotectonic setting of Ediacaran metabasites from the Ossa-Morena Zone (SW Iberia). Int J Earth Sci (Geol Rundsch), 103, 1263–1286 DOI:10.1007/s00531-013-0937-x

Sánchez-Lorda, M.E., Ábalos, B., García de Madinabeitia, S., Eguíluz, L., Gil Ibarguchi, J.I., Paquette, J.L. (2016). Radiometric discrimination of pre-Variscan amphibolites in the Ediacaran *Série Negra* (Ossa-Morena Zone, SW Iberia). Tectonophysics, 681, 31–45. DOI: 10.1016/j.tecto.2015.09.020

Sarmiento, G.N., Piçarra, J.M., Oliveira, J.T. (2000). Conodontes do Silúrico (Superior?)-Devónico nos "Mármores de Estremoz", Sector de Estremoz-Barrancos (Zona de Ossa Morena, Portugal). Implicações estratigráficas e estruturais a nível regional. I Congresso Ibérico de Paleontologia/VIII International Meeting of IGCP 421 (abstract book), Évora, 284-285.

Schäfer, H. J. (1990): Geochronological investigations in the Ossa-Morena Zone, SW Spain. Ph. D. ETH, Zurich: 153 p.

Schäfer, H.J., Gebauer, D., Nägler, Th.F., Von Quadt, A. (1988). U–Pb zircon and Sm–Nd studies of various rock-types of the Ossa-Morena Zone (Southwest Spain). Simposio sobre cinturones orogénicos. I Congreso Español de Geologíapp. 51–57.

Schäfer, H. J., Gebauer, D. Ynagler, Th. F. (1989). Pan-African and Caledonian ages in the Ossa-Morena Zone (Southwest Spain): a U-Pb zircão and Sm-Nd study. Terra Abstracts, 1, 350-351.

Schäfer, H.J., Gebauer, D., Nagler T.F., Eguíluz, L. (1993). Conventional and ion-microprobe U-Pb dating of detrital zircãos of the Tentudía Group (*Série Negra*, SW Spain): implications for zircão systematics, stratigraphy, tectonics and the Precambrian/Cambrian boundary. Contrib Mineral Petrol, 113, 289-299.

Serrano Pinto, M. (1984). Granitóides Caledónicos e Hercínicos na Zona de Ossa-Morena (Portugal) – Nota sobre aspectos geocronológicos. Memórias e Notícias – Universidade de Coimbra, 97, 81-94.

Simancas, J.F., Expósito, I., Azor, A., Martínez Poyatos, D.J., González Lodeiro, F., (2004). From the Cadomian orogenesis to the Early Palaeozoic Variscan rifting in southwest Iberia. Journal of Iberian Geology 30, 53–71.

Stow, D.A.V., Shanmugam, G. (1980). Sequences of structures in finegrained turbidites: comparison of recent deep-sea and ancient flysch sediments. Sediment. Geol., 25 (1-2), 23-42. DOI:10.1016/0037-0738(80)90052-4

Sun S.S., McDonough W.F. (1989). Chemical and isotopic systematics of oceanic basalts: implications for mantle composition and processes. In Magmatism in the Ocean Basins (eds. A. D. Saunders and M. J. Norry, vol. 42.). The Geological Society, 313–345. DOI:10.1144/GSL.SP.1989.042.01.19

Sun, S.S., Nesbht, R. W.Sharaskin, A. Y. (1979). Geochemical characteristics of mid-ocean ridge basalts. Earth and Planetary Science Letters, 44, 119-138. DOI: 10.1016/0012-821X(79)90013-X

Teixeira, C. (1981). Geologia de Portugal. Precâmbrico-Paleozóico. Lisboa, Fundação Calouste Gulbenkian. 629p

Vegas, K. (1968). Sobre la existencia de Precambrico en la Baja Extremadura, Estud, GeoL 24, 85-89.

Vera, J.A., (Eds.), (2004). Geología de España. Sociedad Geológica de España e Instituto Geológico y Minero de España, 884 p.

Walker, R.G. (1976). Facies Models 2. Turbidites and Associated Coarse Clastic Deposits. GeoscienceCanada, 3 (1), 25-36.

Whitney, D.L., Evans, B.W. (2010). Abbreviations for names of rock-forming minerals. American Mineralogist, 95 (1), 185-187. DOI: 10.2138/am.2010.3371

Wood, D.A (1980). The application of a Th-Hf-Ta diagram to problems of tectono-magmatic classification and to establishing the nature of crustal contamination of basaltic lavas of the British Tertiary volcanic province. Earth and Planetary Science Letters, 50, 11–30. DOI: 10.1016/0012-821X(80)90116-8